LBL-28797
Preprint

Lawrence Berkeley Laboratory
UNIVERSITY OF CALIFORNIA

Submitted to Nuclear Physics A

Model for Statistical Properties of Nuclear Systems at Finite Temperature

J. Randrup and E.D. Medeiros

August 1990

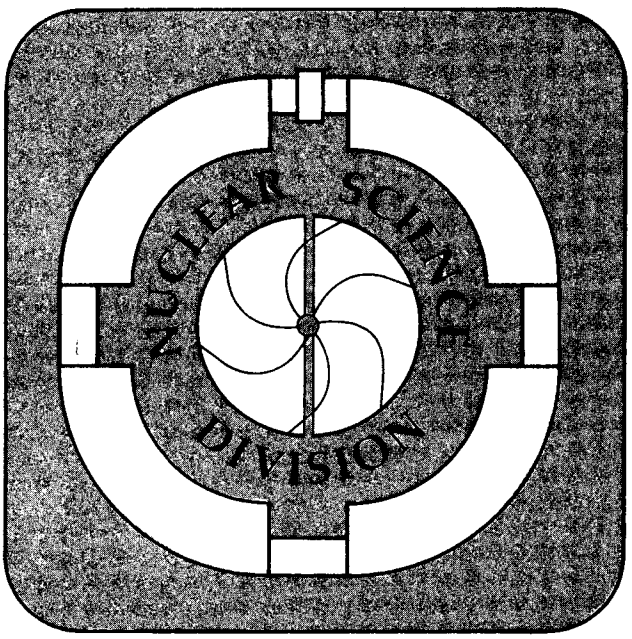

LBL-28797
Copy 2
Bldg. 50 Library.
LOAN COPY
Circulates
for 2 weeks

Prepared for the U.S. Department of Energy under Contract Number DE-AC03-76SF00098.

DISCLAIMER

This document was prepared as an account of work sponsored by the United States Government. While this document is believed to contain correct information, neither the United States Government nor any agency thereof, nor the Regents of the University of California, nor any of their employees, makes any warranty, express or implied, or assumes any legal responsibility for the accuracy, completeness, or usefulness of any information, apparatus, product, or process disclosed, or represents that its use would not infringe privately owned rights. Reference herein to any specific commercial product, process, or service by its trade name, trademark, manufacturer, or otherwise, does not necessarily constitute or imply its endorsement, recommendation, or favoring by the United States Government or any agency thereof, or the Regents of the University of California. The views and opinions of authors expressed herein do not necessarily state or reflect those of the United States Government or any agency thereof or the Regents of the University of California.

LBL-28797

Model for Statistical Properties of Nuclear Systems at Finite Temperature*

Jørgen Randrup
Nuclear Science Division, Lawrence Berkeley Laboratory
University of California, Berkeley, California 94720

Emil de Lima Medeiros†
Centro Brasileiro de Pesquisas Físicas - CBPF
Conselho Nacional de Desenvolvimento Científico e Tecnológico - CNPq
22.290 Rio de Janeiro, RJ - Brazil

August 31, 1990

ABSTRACT:

We develop a general model with which the statistical properties of nuclear systems can be addressed. Within a semi-classical treatment, using a new finite-range effective nucleon-nucleon interaction depending on both momentum and density, we derive expressions for the free energy as a functional of the specified spatial density distribution, at a given temperature. We explore a family of interactions that all yield the same reasonable properties of nuclear systems at zero temperature, but differ with regard to the effective mass of the nucleon. In order to make contact with other approaches, we calculate the equation of state for uniform isosymmetric matter and the associated phase diagram; the limiting temperature is 12-13 MeV, while the critical temperature is around 16 MeV. The response of uniform matter to density ripples is studied for a range of temperatures and densities and the calculated critical wave length is found to be sensitive to the new parameter governing the effective mass.

*This work was supported in part by the Director, Office of Energy Research, Office of High Energy and Nuclear Physics, Nuclear Physics Division of the U.S. Department of Energy under Contract No. DE-AC03-76SF00098.

†Fellow, Brazilian Conselho Nacional de Desenvolvimento Cioentífico e Tecnológico - CNPq, Contract No. 20.2057/89.5.
Present address: Nuclear Science Division, Lawrence Berkeley Laboratory
University of California, Berkeley, California 94720.

1 Introduction

In the present work, we develop a self-consistent microscopic nuclear model that, for a specified temperature, yields the statistical weight for an arbitrary spatial distribution of the nucleons. Our goal is to develop a general theoretical tool with which to address finite-temperature non-equilibrium systems, such as those produced transiently in nuclear collisions at intermediate energies. In addition to its expected utility for heavy-ion physics, the model may also be useful in astrophysics, particularly for studying the structure of non-uniform matter at subsaturation densities.

The developed model extends or improves earlier treatments by various groups. About twenty years ago, Myers and Swiatecki [1] formulated a simple model for average nuclear properties. It employed an effective nucleon-nucleon interaction of the form first considered by Seyler and Blanchard [2], namely a Yukawa force modulated by a quadratic momentum dependence, and it was solved self-consistently within the Thomas-Fermi approximation. By fitting its four parameters to the binding energy, density, surface energy, and symmetry energy of standard nuclear matter, Myers and Swiatecki obtained a good overall reproduction of nuclear binding energies and density distributions, apart from irregularities associated with the single-particle structure (shell effects). The most striking shortcoming of the model was that the effective nucleon mass was significantly too small ($\approx 0.38m$), leading to a too rapid energy dependence of the optical potential. This deficiency is inherent in the Seyler-Blanchard interaction because the nuclear saturation is produced exclusively by the momentum dependence. Another, less important, discrepancy was a somewhat too abrupt fall-off of the nuclear density distributions. This feature is characteristic of the Thomas-Fermi approximation which is relatively inaccurate in the surface region.

The Seyler-Blanchard model was subsequently extended to finite temperatures by Küpper *et al.* [3] in a general study of thermostatic properties of isosymmetric (and uniform) nuclear matter. These authors recognized that the unrealistic value of the effective mass might render their results somewhat unreliable. However, no satisfactory remedy for this important problem was found, until recently when Myers and Swiatecki added an explicit density dependence to the effective interaction so that the strength of the momentum dependence can be reduced [4]. With this generalization of the Seyler-Blanchard interaction, the observed energy dependence of the optical potential (hence the effective mass) can now also be well reproduced. (A further term with an inverse momentum dependence can be added in order to also obtain good density profiles [4].) The resulting model yields a very good reproduction of average nuclear properties, such as binding energies, fission barriers, and density distributions. It is expected to be accurate for even very small or very deformed nuclei, and to be reliable for extrapolating to extremely large hypothetical nuclei, including systems with arbitrary neutron excess and arbitrary geometries, such as those that sometimes arise in astrophysical applications. Thus, with the model firmly anchored in observed properties of nuclei, it is of interest to broaden the scope to also encompass finite temperatures. Our present work can be regarded as such an extension.

It should be emphasized that numerous other researchers have studied the nuclear equation of state, and with a variety of approaches. In this presentation we

mention only a few instructive examples. In particular, for astrophysical purposes, Lattimer and Ravenhall studied the bulk properties of nuclear matter on the basis of a Skyrme interaction.[5] This approach is conceptually similar to the above-mentioned earlier work by Küpper *et al.*[3], and hence to ours, but differs primarily in the choice of interaction. One difference is that the Skyrme interaction used in ref. [5] has more adjustable parameters, as well as an explicit density dependence, and so it can be brought to fit more known nuclear properties. Another important feature of the Skyrme interaction is its vanishing range, which simplifies the calculations considerably, since the thermodynamic distributions are then functions rather than functionals of the basic particle and kinetic densities. A finite-range interaction is particularly difficult to treat when the densities deviate from uniformity. While the range of the force may be less important when only bulk properties are studied, as in ref. [5], the relative smallness of the systems generated in nuclear collisions and their irregular appearance demand that the finite range of the nuclear forces be taken into account. Our work is primarily aimed at heavy-ion related problems and it is a special advantage of our model that it provides the statistical weight for *arbitrary* density distributions, with the finite interaction range incorporated consistently.

Many calculations of the nuclear equation of state have been made on the basis of microscopic models. An often quoted example is the work by Friedman and Pandharipande [6], who performed a variational calculation of the equation of state based on a realistic Hamiltonian with fitted two- and three-nucleon interaction terms. Though such calculations have the advantage of being based on independently known microscopic properties (such as the NN scattering cross section), they are fairly tedious and, in particular, they are not easily extended to systems with non-uniform density distributions. We shall make detailed comparisons with the microscopic calculations of ref. [6], in order to assess the quantitative utility of the approach.

In order to provide a useful tool for quantitative studies of the statistical properties of finite-temperature non-uniform nuclear systems, we have undertaken to develop a conceptually simple model of rather general applicability. Working within the semi-classical (Thomas-Fermi) mean-field approximation, we describe the system in terms of its reduced one-particle phase-space distribution. The individual nucleons interact via a Yukawa potential whose strength depends on both momentum and density. The specific form is the density-dependent generalization of the Seyler-Blanchard interaction recently introduced by Myers and Swiatecki [4]. For any given temperature, the model yields the statistical weight associated with an arbitrary spatial density distribution and, consequently, the statistical properties of non-uniform nuclear matter can be addressed, including fluctuations. Moreover, since the model treats the liquid and vapor phases on an equal footing, it presents an especially useful tool for studying phenomena associated with the nuclear liquid-gas phase transition. Finally, it should be stressed that the model is expected to be quantitatively useful, since it reproduces known macroscopic nuclear properties, such as binding and deformation energies, density shapes and profiles, and effective mass and optical potentials [1, 4].

The formal tools developed to treat models of the generalized Seyler-Blanchard type are described in section 2. Then, in section 3, we calculate the equation of state of uniform nuclear matter for a variety of parameter sets, both in order to make

contact with earlier studies and to determine the sensitivity to the specific interaction. We also calculate the associated phase diagrams and make detailed comparisons with the microscopic results of ref. [6], to permit a general assessment of the model. A first application of the model to non-uniform distributions is made in section 4, where the response of nuclear matter to density ripples is explored. In section 5 we summarize and outline expected further developments and applications. Appendix A describes the Fermi-Dirac moments introduced to achieve fast and convenient computation, and appendix B describes an efficient algorithm developed for carrying out the necessary convolutions.

2 Model

The present work is carried out within a semi-classical framework, so that a nucleon can be characterized by its position $\mathbf{r}$ and momentum $\mathbf{p}$. Furthermore, we restrict the formulation to nuclear systems with spin-isospin symmetry, so that each single-particle orbital has a degeneracy of $g = 4$. It is straightforward to relax this restriction. Finally, in this initial work we consider only the nuclear part of the interaction and thus omit the Coulomb force entirely. However, when studying the geometrical organization of subsaturation nuclear matter it is essential to include the Coulomb force.

2.1 Seyler-Blanchard model

Seyler and Blanchard [2] introduced an effective interaction with an explicit momentum dependence of quadratic form,

$$V_{12}^{\mathrm{SB}} = -C \, \frac{\mathrm{e}^{-r_{12}/a}}{r_{12}/a} \, (1 - \frac{p_{12}^2}{b^2}) \, , \tag{1}$$

where $\mathbf{r}_{12} = \mathbf{r}_1 - \mathbf{r}_2$ and $\mathbf{p}_{12} = \mathbf{p}_1 - \mathbf{p}_2$. It has three parameters: the range a of the spatial form factor (taken to be a Yukawa function), the characteristic momentum b, and the overall interaction strength C; it is convenient to also introduce the characteristic kinetic energy $T = b^2/2m$, where m is the free nucleon mass. Reasonable values of these parameters can be determined by demanding a reproduction of the nuclear-matter saturation density and energy, as well as the nuclear surface energy. The quality of these fits is similar to what can be obtained with Skyrme-type effective interactions that depend only on density.

In their original study, Myers and Swiatecki [1] determined the parameters as a=0.62567 fm, T=82.030 MeV, and C=328.61 MeV. These values lead to a saturation density of $\rho_0 = 0.1365$ fm^{-3}, corresponding to a Fermi energy of $T_F = 33.138$ MeV, and the compressibility coefficient, which is given by $K = 6T_F(4\pi a^3 \rho_0 C/T - 1/5)$, follows as $K = 294.60$ MeV. Later on, von Groote [7] refitted the parameters and obtained a=0.557 fm, T=89.274 MeV, and C=435.1 MeV. The associated value $\rho_0 = 0.153$ fm^{-3} (*i.e.* T_F=35.76 MeV) is in somewhat better accordance with experiment, and the corresponding compressibility $K = 304.5$ MeV is still a fairly

reasonable value. In the present study, we shall adopt these latter values as the standard parameter set, because of the better saturation density obtained. In their recent work, Myers and Swiatecki [4] have determined new preliminary parameters leading to $\rho_0 = 0.1645$ fm^{-3} (T_F=37.679 MeV) and $K = 301.27$ MeV, which are probably somewhat better values. However, these values have been determined for an interaction that has an additional term with an inverse momentum dependence and hence they do not necessarily apply to our present model. When improved parameters are available for the standard interaction (1), it will be preferable to adopt those values to ensure an optimum reproduction of known nuclear properties.

With the interaction specified as in (1), the many-body Hamiltonian follows. We shall employ the semi-classical mean-field approximation in our further considerations. The motion of an individual nucleon is then governed by an effective one-body Hamiltonian $h(\mathbf{r},\mathbf{p})$. Due to the quadratic momentum dependence of the interaction, this quantity is of the simple standard form

$$h(\mathbf{r},\mathbf{p}) \;=\; \frac{p^2}{2B(\mathbf{r})} + U(\mathbf{r}) \;, \tag{2}$$

where $B(\mathbf{r})$ is the effective mass and $U(\mathbf{r})$ is the effective static potential, both dependent on the position $\mathbf{r}$ of the nucleon [8] (see eqs. (9-10)).

In the mean-field approximation, the state of the system is specified by its one-particle phase-space density distribution $f(\mathbf{r},\mathbf{p})$, and any state is characterized in terms of its spatial distribution $\rho(\mathbf{r})$, in addition to a given temperature τ, which governs the diffuseness of the local momentum distribution. Thus, for given $\rho(\mathbf{r})$ and τ, the occupancy in phase space is given by the Fermi-Dirac distribution

$$f(\mathbf{r},\mathbf{p}) \;=\; \left[1+\mathrm{e}^{\beta(h-\mu)}\right]^{-1} \;=\; \left[1+\mathrm{e}^{p^2/2B\tau-\alpha}\right]^{-1} \;. \tag{3}$$

Here $h(\mathbf{r},\mathbf{p})$ is the single-particle Hamiltonian (2) and $\alpha(\mathbf{r}) = \beta(\mu - U(\mathbf{r}))$ is the local fugacity, with $\beta\tau = 1$. The chemical potential $\mu(\mathbf{r})$ is employed as a position-dependent parameter that will be adjusted so that the specified local density $\rho(\mathbf{r})$ is obtained.

This latter quantity, the nucleon density distribution $\rho(\mathbf{r})$, and the associated kinetic density $\kappa(\mathbf{r})$, are given in terms of $f(\mathbf{r},\mathbf{p})$ as

$$\rho(\mathbf{r}) \;=\; g\int \frac{d\mathbf{p}}{h^3}\, f(\mathbf{r},\mathbf{p}) = F_{\frac{1}{2}}(\alpha(\mathbf{r}))\;\rho_\tau(\mathbf{r}) \;, \tag{4}$$

$$\kappa(\mathbf{r}) \;=\; g\int \frac{d\mathbf{p}}{h^3}\,\frac{p^2}{b^2}\, f(\mathbf{r},\mathbf{p}) = \frac{2B(\mathbf{r})\tau}{b^2}\; F_{\frac{3}{2}}(\alpha(\mathbf{r}))\;\rho_\tau(\mathbf{r}) \;. \tag{5}$$

Here we have employed the Fermi-Dirac moments $F_n(\alpha)$ discussed in appendix A. These convenient dimensionless quantities are functions of the fugacity α. It is also convenient to define the thermal density $\rho_\tau(\mathbf{r}) = 2\pi g(2B(\mathbf{r})\tau/h^2)^{3/2}$.

The total energy of the system can be written on the form $E = \int d\mathbf{r}e(\mathbf{r})$, where $e(\mathbf{r})$ is the energy density. This quantity is composed of several distinct terms: $e =$

$e_{\rm kin} + e_0 + e_2$, where

$$
\begin{aligned}
e_{\rm kin}(\mathbf{r}) &= g\int \frac{d\mathbf{p}}{h^3}\, f(\mathbf{r},\mathbf{p})\, \frac{p^2}{2m} = T\kappa(\mathbf{r})\ , \\
e_0(\mathbf{r}_1) &= -\frac{C}{2} g \int \frac{d\mathbf{r}_2 d\mathbf{p}_2}{h^3}\, f(\mathbf{r}_2,\mathbf{p}_2)\, \frac{\mathrm{e}^{-r_{12}/a}}{r_{12}/a} = -\frac{C}{2}\mathcal{R}(\mathbf{r}_1)\rho(\mathbf{r}_1)\ , \qquad (6)\\
e_2(\mathbf{r}_1) &= \frac{C}{2} g \int \frac{d\mathbf{r}_2 d\mathbf{p}_2}{h^3}\, f(\mathbf{r}_2,\mathbf{p}_2)\, \frac{\mathrm{e}^{-r_{12}/a}}{r_{12}/a}\, \frac{p_{12}^2}{b^2} = \frac{C}{2}\left(\mathcal{K}(\mathbf{r}_1)\rho(\mathbf{r}_1) + \mathcal{R}(\mathbf{r}_1)\kappa(\mathbf{r}_1)\right)\ .
\end{aligned}
$$

We have here employed the auxiliary functions [8]

$$
\mathcal{R}(\mathbf{r}_1) = \int d\mathbf{r}_2\, \frac{\mathrm{e}^{-r_{12}/a}}{r_{12}/a}\, \rho(\mathbf{r}_2) \asymp 4\pi a^3 \rho\ , \qquad (7)
$$

$$
\mathcal{K}(\mathbf{r}_1) = \int d\mathbf{r}_2\, \frac{\mathrm{e}^{-r_{12}/a}}{r_{12}/a}\, \kappa(\mathbf{r}_2) \asymp 4\pi a^3 \kappa\ . \qquad (8)
$$

They are obtained from the basic densities ρ and κ by convoluting with the Yukawa form factor entering in the Seyler-Blanchard interaction (1). Physically, $\mathcal{R}(\mathbf{r})$ represents the number of nucleons within reach of the force, at the specified location $\mathbf{r}$, and $\mathcal{K}(\mathbf{r})$ is an analogous quantity. The symbol $\asymp$ has been adopted to indicate relations pertaining to uniform matter, in which the densities are independent of position.

By performing a variation of the total energy E with respect to the local density $\rho(\mathbf{r})$, it is easy to derive the expressions

$$
\frac{m}{B(\mathbf{r})} = 1 + \frac{C}{T}\mathcal{R}(\mathbf{r}) \asymp 1 + \frac{C}{T} 4\pi a^3 \rho\ , \qquad (9)
$$

$$
U(\mathbf{r}) = -C\left(\mathcal{R}(\mathbf{r}) - \mathcal{K}(\mathbf{r})\right) \asymp -4\pi a^3 C(\rho - \kappa) \qquad (10)
$$

for the effective mass B and the static potential U.

These latter relations close the system of equations. We now proceed as follows. For a fixed temperature τ, assume that the spatial distribution of nucleons is specified. For the given density $\rho(\mathbf{r})$, the auxiliary function $\mathcal{R}$ can be calculated by performing the convolution as defined in (7). This in turn determines the effective mass $B(\mathbf{r})$ as a function of the position $\mathbf{r}$. The relation (4) for the density $\rho(\mathbf{r})$ can then be solved for the local fugacity $\alpha(\mathbf{r})$, using the Fermi-Dirac moments described in Appendix A. Subsequently, the equation (5) yields the kinetic density $\kappa(\mathbf{r})$, and the auxiliary function $\mathcal{K}(\mathbf{r})$ follows from (8). In this manner we can obtain all the quantities needed to evaluate the energy density (6) and the effective single-particle Hamiltonian (2). This solution method is very efficient and makes it possible to quickly calculate the self-consistent many-particle state associated with any specified density distribution $\rho(\mathbf{r})$.

In order to determine the thermodynamic quantities, we need to calculate the entropy $S[\rho] = \int d\mathbf{r} s(\mathbf{r})$, in addition to the energy E obtained as described above. The entropy density $s(\mathbf{r})$ can be obtained from the standard expression for a Fermi-Dirac gas,

$$
s(\mathbf{r}) = g\int \frac{d\mathbf{p}}{h^3}\left[\frac{\ln(1+\mathrm{e}^{\beta(\epsilon-\mu)})}{1+\mathrm{e}^{\beta(\epsilon-\mu)}} + \frac{\ln(1+\mathrm{e}^{\beta(\mu-\epsilon)})}{1+\mathrm{e}^{\beta(\mu-\epsilon)}}\right] = G_{\frac{1}{2}}(\alpha(\mathbf{r}))\ \rho_\tau(\mathbf{r})
$$

$$= \left(\frac{5}{3}F_{\frac{3}{2}}(\alpha) - \alpha F_{\frac{1}{2}}(\alpha)\right)\rho_\tau = \frac{5}{3}\frac{b^2}{2B\tau}\kappa - \alpha\rho \ , \tag{11}$$

where the universal function $G_n(\alpha)$ is defined in Appendix (A). Thus $s(\mathbf{r})$ is also expressible in terms of the basic densities $\rho(\mathbf{r})$ and $\kappa(\mathbf{r})$.

The statistical weight of the system characterized by a specified density distribution $\rho(\mathbf{r})$ is given by

$$W[\rho] = \mathrm{e}^{-\beta F[\rho]} \ , \tag{12}$$

where F denotes the free energy of the system. This key quantity is a function of the temperature τ and a functional of the spatial density $\rho(\mathbf{r})$. Having calculated the energy E and the entropy S as described above, the free energy readily follows as

$$F[\rho] = E[\rho] - \tau S[\rho] \ . \tag{13}$$

(More generally, one may consider the local free energy per nucleon, $\phi(\mathbf{r}) = \epsilon(\mathbf{r}) - \tau\sigma(\mathbf{r})$, where $\epsilon = e/\rho$ is the local energy per nucleon and $\sigma = s/\rho$ is the local entropy per nucleon.) We note that the ground state of the system can be determined by minimizing the energy E, which is a relatively simple task. However, for a finite temperature, the equilibrium configuration is obtained by minimizing the free energy F, which is more complicated because of the entropy contribution $-\tau S$.

In order to calculate the equation of state, we need the pressure P. In general, the local pressure can be obtained from the thermodynamic relation $P(\mathbf{r}) = \rho^2(\partial\phi/\partial\rho)_\tau$. In the present study, we shall consider the pressure only in the context of uniform systems, in which case we have $P\Omega = \rho(\partial F/\partial\rho)_\tau - F$, where Ω is the volume of the uniform system. We may thus calculate the pressure as

$$P = \left(\rho(\frac{\partial e}{\partial\rho})_\tau - e\right) - \tau\left(\rho(\frac{\partial s}{\partial\rho})_\tau - s\right) \ . \tag{14}$$

We note that $P = 0$ iff $(\partial\phi/\partial\rho)_\tau = 0$, so that the pressure vanishes in any equilibrium state, as it should be.

2.2 Generalized interaction

In a concurrent study of macroscopic nuclear properties [4], Myers and Swiatecki have introduced a modified Seyler-Blanchard interaction, in which part of the explicit momentum-dependence is replaced by a density dependence. This modification is made in order to improve the reproduction of the optical potential, while preserving the overall good reproduction of the many other average nuclear properties, such as binding energies, fission barriers, and density distributions. Although that study is limited to zero temperature, and the specific modification correspondingly limited in scope, it is easy to generalize the idea to arbitrary situations. Because of the resulting very good global description of a large variety of static nuclear properties [4], we find it especially interesting to include this interaction in our present study.

For this purpose, we generalize the Myers-Swiatecki modification to arbitrary phase-space distributions as follows,

$$V_{12}^{\chi} = -C\,\frac{e^{-r_{12}/a}}{r_{12}/a}\left[1-\bar{\chi}\frac{p_{12}^2}{b^2}-\chi\frac{\kappa_0}{\rho_0}\left((\frac{\rho_1}{\rho_0})^{\frac{2}{3}}+(\frac{\rho_2}{\rho_0})^{\frac{2}{3}}\right)\right] , \tag{15}$$

where ρ_i means $\rho(\mathbf{r}_i)$ and $\bar{\chi}=1-\chi$ for convenience. The (arbitrary) reference density ρ_0 is chosen as the saturation density of the model for zero temperature, and κ_0 is the corresponding value of the kinetic density κ. It should be noted that the standard Seyler-Blanchard interaction (1) is recovered for $\chi=0$. Because of the explicit density dependence brought in by the new interaction term proportional to the parameter χ, the treatment is more complicated and we therefore sketch the method employed.

It is convenient to introduce the pseudo-kinetic density $\tilde{\kappa}(\mathbf{r})=\kappa_0(\rho(\mathbf{r})/\rho_0)^{5/3}$, and the associated auxiliary function $\tilde{\mathcal{K}}(\mathbf{r})$ defined in analogy with (8). We may then also introduce $\kappa_{\text{eff}}=\bar{\chi}\kappa+\chi\tilde{\kappa}$. The energy density may then be written $e_\chi=e_{\text{kin}}+e_0+e_{\text{eff}}$, with $e_{\text{eff}}=\bar{\chi}e_2+\chi\tilde{e}_2$, where e_{kin}, e_0, and e_2 are given in (6) and

$$\begin{aligned}\tilde{e}_2(\mathbf{r}_1) &= \frac{C}{2}g\int\frac{d\mathbf{r}_2d\mathbf{p}_2}{h^3}\,f(\mathbf{r}_2,\mathbf{p}_2)\,\frac{e^{-r_{12}/a}}{r_{12}/a}\left(\frac{\tilde{\kappa}(\mathbf{r}_1)}{\rho(\mathbf{r}_1)}+\frac{\tilde{\kappa}(\mathbf{r}_2)}{\rho(\mathbf{r}_2)}\right)\\ &= \frac{C}{2}\left(\tilde{\mathcal{K}}(\mathbf{r}_1)\rho(\mathbf{r}_1)+\mathcal{R}(\mathbf{r}_1)\tilde{\kappa}(\mathbf{r}_1)\right)\asymp C4\pi a^3\rho\tilde{\kappa}\sim\rho^{8/3} .\end{aligned} \tag{16}$$

For a uniform system we then have

$$e_\chi \asymp \frac{b^2}{2B}\kappa-\frac{C}{2}4\pi a^3\rho(\rho-2\chi\tilde{\kappa}) , \tag{17}$$

$$f_\chi \asymp -\frac{2}{3}\frac{b^2}{2B}\kappa-\frac{C}{2}4\pi a^3\rho(\rho-2\chi\tilde{\kappa})-\mu\rho , \tag{18}$$

where $f_\chi=\phi\rho$ is the free-energy density.

In order to obtain the expression for the effective single-particle Hamiltonian h_χ, the system is subjected to a variation $\delta f(\mathbf{r},\mathbf{p})=h^3\delta(\mathbf{r}-\mathbf{r}_0)\delta(\mathbf{p}-\mathbf{p}_0)$, which corresponds to the introduction of a test nucleon at the point $(\mathbf{r}_0,\mathbf{p}_0)$ in phase space. The induced changes in the various densities are then $\delta\rho(\mathbf{r})=\delta(\mathbf{r}-\mathbf{r}_0)$, $\delta\kappa(\mathbf{r})=(p_0/b)^2\delta\rho(\mathbf{r})$, and $\delta\tilde{\kappa}(\mathbf{r})=(5\tilde{\kappa}/3\rho)\delta\rho(\mathbf{r})$. Consequently, the induced change in the total energy E is

$$\delta E=\int d\mathbf{r}\left[\frac{p_0^2}{m}\left(1+\bar{\chi}\frac{C}{T}\mathcal{R}(\mathbf{r})\right)-C\left(\mathcal{R}(\mathbf{r})-\mathcal{K}_{\text{eff}}(\mathbf{r})-\frac{5}{3}\chi\frac{\tilde{\kappa}(\mathbf{r})}{\rho(\mathbf{r})}\mathcal{R}(\mathbf{r})\right)\right]\,\delta\rho(\mathbf{r}) . \tag{19}$$

Since δE can be identified with the effective single-particle Hamiltonian h_χ, we see that this quantity is still of the form (2), but with modified expressions for the effective mass and potential,

$$\frac{m}{B_\chi(\mathbf{r})} = 1+\bar{\chi}\frac{C}{T}\mathcal{R}(\mathbf{r}) \asymp 1+\bar{\chi}\frac{C}{T}4\pi a^3\rho , \tag{20}$$

$$U_\chi(\mathbf{r}) = -C\left(\mathcal{R}(\mathbf{r})-\mathcal{K}_{\text{eff}}(\mathbf{r})-\frac{5}{3}\chi\frac{\tilde{\kappa}(\mathbf{r})}{\rho(\mathbf{r})}\mathcal{R}(\mathbf{r})\right) \asymp -4\pi a^3C(\rho-\kappa_{\text{eff}}-\frac{5}{3}\chi\tilde{\kappa}) .$$

It is evident that for zero temperature the resulting energy density $e_\chi(\mathbf{r})$ is in fact independent of the parameter χ, since then $\tilde{\kappa} = \kappa$. Consequently, all zero-temperature results derived on the basis of $e(\mathbf{r})$ (such as binding energies, fission barriers, and density profiles) remain unaffected by the modification.

The fact that the effective single-particle Hamiltonian depends on the parameter χ has direct implications for the optical potential. Moreover, because the single-particle energy enters in the Fermi-Dirac occupancy coefficients (3), the self-consistent solution also depends on χ, so that in general the finite-temperature properties of the system are sensitive to this parameter. We shall exhibit these two effects below.

2.3 Optical potential

The optical potential $U^{\rm opt}(\mathbf{r}, E)$ is obtained by rewriting the effective Hamiltonian (2) on the form $H^{\rm opt} = p^2/2m + U^{\rm opt}$. This yields the result

$$U^{\rm opt}(\mathbf{r}) = \frac{B_\chi(\mathbf{r})}{m}\left(U_\chi(\mathbf{r}) + \bar{\chi}\frac{C}{T}\mathcal{R}(\mathbf{r})E\right) . \tag{21}$$

As discussed in ref. [4], the energy dependence of the optical potential is rather poorly reproduced by the standard Seyler-Blanchard interaction ($\chi = 0$), as illustrated by the fact that the effective nucleon mass comes out as $B_0 = 0.3817\ m$. By contrast, as was already noted by Myers and Swiatecki [4], a value $\chi \approx 0.75$ leads to a nearly perfect reproduction of the experimental values, in particular the effective mass is $B_0 = 0.7118\ m$. In our present study, we adopt this latter value as the standard value; it yields approximately the same ratio between the two χ-dependent terms in the interaction as obtained in ref. [4].

It should be noted that the replacement of the effective Hamiltonian (2) with the optical-model Hamiltonian $H^{\rm opt}$ modifies the equations of motion and thus leads to a different time evolution $(\mathbf{r}^{\rm opt}(t), \mathbf{p}^{\rm opt}(t))$ of an individual nucleon. However, the effect merely corresponds to a distortion of the time parameter, so we may write

$$\mathbf{r}^{\rm opt}(t) = \mathbf{r}(t^{\rm opt}) \ , \ \mathbf{p}^{\rm opt}(t) = \mathbf{p}(t^{\rm opt}) \ , \tag{22}$$

where $(\mathbf{r}(t), \mathbf{p}(t))$ is the trajectory obtained by solving Hamilton's equations for the effective Hamiltonian (2) and the progression of the stretched time $t^{\rm opt}(t)$ is determined by the differential equation $dt^{\rm opt}/dt = B/m$. Thus, within the semi-classical approximation, both the scattering angle and the phase shift will be correctly reproduced by the optical potential, even though the speed of the nucleon is lowered in the medium. This correspondence is generally expected for time-independent scenarios, since the introduction of the optical potential implicitly assumes that the energy of the particle remains constant in time.

2.4 Pressure

Employing the formula (14), we here derive the expression for the pressure in a uniform system subject to the generalized Seyler-Blanchard interaction (15).

For a uniform system, the expression for the energy density is

$$e_\chi \asymp T\kappa - \frac{C}{2}4\pi a^3\rho(\rho - 2\kappa_{\text{eff}}) \ . \tag{23}$$

Therefore,

$$\rho(\frac{\partial e_\chi}{\partial \rho})_\tau = \frac{b^2}{2B_\chi}\rho(\frac{\partial \kappa}{\partial \rho})_\tau + U_\chi \rho \ , \tag{24}$$

where it has been used that $\tilde{\kappa} \sim \rho^{5/3}$. The pressure may then be written as

$$\begin{aligned} P &\asymp \frac{b^2}{2m}(\rho\frac{\partial \kappa}{\partial \rho} - \kappa) + C4\pi a^3\rho(\rho\frac{\partial \kappa_{\text{eff}}}{\partial \rho} - \kappa_{\text{eff}}) - \frac{C}{2}4\pi a^3\rho(\rho - 2\kappa_{\text{eff}}) - \tau(\rho\frac{\partial s}{\partial \rho} - s) \\ &= \frac{b^2}{2B_\chi}(\rho\frac{\partial \kappa}{\partial \rho} - \kappa) - \frac{C}{2}4\pi a^3\rho(\rho - 2\kappa_{\text{eff}} - \frac{4}{3}\chi\tilde{\kappa}) - \tau(\rho\frac{\partial s}{\partial \rho} - s) \ , \end{aligned} \tag{25}$$

where the derivatives should be carried out at the fixed temperature τ. The only remaining problem is now to evaluate the derivatives $\partial\kappa/\partial\rho$ and $\partial s/\partial\rho$.

These quantities can be expressed in terms of the universal moments discussed in appendix A. First note that the density dependence of the fugacity can be obtained by performing a differentiation of the relation (4) with respect to ρ,

$$\rho(\frac{\partial \alpha}{\partial \rho})_\tau = (\frac{5}{2} - \frac{3}{2}\frac{B_\chi}{m})\ \frac{F_{\frac{1}{2}}(\alpha)}{F'_{\frac{1}{2}}(\alpha)} \ . \tag{26}$$

Consequently,

$$(\frac{\partial \kappa}{\partial \rho})_\tau = \frac{3B_\chi\tau}{b^2}\ (\frac{5}{2} - \frac{3}{2}\frac{B_\chi}{m})\ \frac{F_{\frac{1}{2}}(\alpha)}{F'_{\frac{1}{2}}(\alpha)} - (\frac{5}{2} - \frac{5}{2}\frac{B_\chi}{m})\ \frac{\kappa}{\rho} \ . \tag{27}$$

The density dependence of the entropy density follows similarly,

$$(\frac{\partial s}{\partial \rho})_\tau = (\frac{5}{2} - \frac{3}{2}\frac{B_\chi}{m})\ \frac{G'_{\frac{1}{2}}(\alpha)}{F'_{\frac{1}{2}}(\alpha)} - (\frac{3}{2} - \frac{3}{2}\frac{B_\chi}{m})\ \frac{s}{\rho} \ . \tag{28}$$

The various universal moments are discussed in appendix A; they can be tabulated ahead of time and so the calculation of the pressure is rather fast.

2.5 Maxwell relations

It should be recognized that the approach taken automatically guarantees that the developed statistical model is thermodynamically consistent. This is most easily verified by checking that the appropriate Maxwell relations hold. In the present model, we specify the system by its temperature τ and density $\rho(\mathbf{r})$. Thermodynamic considerations apply in the limit of large uniform systems. For such a system, specifying the density ρ is equivalent to specifying the volume V within which the system is enclosed. Thus, the proper thermodynamic variables are temperature and volume and,

consequently, the appropriate thermodynamic potential is the Helmholtz free energy $F = E - \tau S$, in accordance with what we have used. The corresponding Maxwell relations then read

$$P = -\left(\frac{\partial F}{\partial V}\right)_\tau \ , \ S = -\left(\frac{\partial F}{\partial \tau}\right)_V \ . \tag{29}$$

Using the displayed expressions for energy, entropy, and pressure, together with the properties of the Fermi-Dirac moments given in Appendix A, it is relatively easy to verify that the above Maxwell relations indeed hold. Of course, the other thermodynamic potentials (*e.g.* the Gibbs potential), and associated Maxwell relations, can then be obtained by the standard transformations.

3 Uniform matter

With the model described above, we now survey the thermostatic properties of nuclear matter. Thus, we consider an infinite system held at a uniform density ρ and kept at a specified temperature τ. The principal purpose of this undertaking is to make contact with the existing calculations of these properties. We wish to emphasize that the motivation for our present work is not to reconsider uniform matter, but to establish a simple and reasonable basis for treating general configurations, which are hard to address in more refined approaches.

In fig. 1 we show the energy per nucleon, $\epsilon = E/A$, as a function of the density ρ. It should be noted that the minimum in this curve shifts outwards towards denser systems as the temperature is increased. This is a consequence of the momentum dependence: for a fixed temperature, the relative diffuseness of the Fermi surface is smaller at higher density, and so the balance between attraction and repulsion is achieved at a higher density. It can be seen that the isotherms are moved up considerably as χ is increased from zero (the pure Seyler-Blanchard case) to the realistic value $\chi = 0.75$. (We recall that all values of χ yield the same results at zero temperature.)

The entropy per nucleon, $\sigma = S/A$, is shown in fig. 2. The entropy decreases steadily with increasing density, because of the general increase with volume of the entropy of a gas. This effect counteracts the behavior of the energy and results in a free energy $F = E - \tau S$ that peaks at a density below saturation, in accordance with the ordinary experience that a body expands when heated. Again we note a significant upwards displacement of the isotherms for $\chi = 0.75$.

3.1 Equation of state

We now turn to the *equation of state* for uniform matter. This key quantity can be expressed as the relationship $P(\rho, \tau)$, *i.e.* the pressure as a function of density and temperature. This quantity is given in (14) and is shown in fig. 3, for $\chi = 0$ and $\chi = 0.75$, using the von Groote parameter values. The zero-temperature results are identical and the corresponding curve increases through $P = 0$ at the saturation density $\rho_0 = 0.153$ fm^{-3}. A quantity of particular interest in connection

with intermediate-energy nuclear reactions is the *limiting temperature* $\tau_{\rm lim}$, defined as the highest value of τ for which the pressure can be negative. For $\tau < \tau_{\rm lim}$ self-cohesive nuclear systems may occur and so $\tau_{\rm lim}$ can be regarded as the maximum temperature for which nuclei can exist. (The limiting temperature is expected to be lower for actual nuclei, due to surface and Coulomb effects.) In fig. 4 is shown the limiting temperature $\tau_{\rm lim}$ and the corresponding density $\rho_{\rm lim}$ as functions of χ. We note that $\tau_{\rm lim}$ decreases up to $\chi \approx 0.5$ and then increases more rapidly. As a result of this behavior, the value $\tau_{\rm lim} = 13.009$ resulting at $\chi = 0.75$ is very similar to the value $\tau_{\rm lim} = 12.998$ MeV obtained with $\chi = 0$, although there is a significant sensitivity of $\tau_{\rm lim}$ to χ near $\chi = 0.75$. The limiting density decreases monotonically from $\rho_{\rm lim} = 0.095$ at $\chi = 0$ to $\rho_{\rm lim} = 0.085$ at $\chi = 0.75$, and the sensitivity is very small near $\chi = 0.75$. As shown by the dashed curves, the behavior obtained with the original Myers-Swiatecki parameters is qualitatively similar, but shifted towards lower temperatures by about 0.60 MeV and lower densities by about 0.010 fm^{-3}.

Also indicated in fig. 4 are the values of temperature and density associated with the *critical point*, at which the maximum and minimum in the pressure curve coalesce into a turning point. For temperatures below critical two distinct phases of nuclear matter coexist, usually referred to as the liquid and the vapor phases. The χ dependence of the critical point is qualitatively similar to the dependence of the limiting values discussed above, with the temperatures shifted upwards by about 4.0 MeV and the densities reduced by about 0.025 fm^{-3}.

3.2 Phase diagram

The equation of state, as depicted in fig. 3, enables us to construct a phase diagram for nuclear matter. The result is shown in fig. 5. In the $\rho - \tau$ plane, the region of phase coexistence is bounded by a parabola-like curve starting at the origin $(0,0)$, peaking at the critical point $(\rho_{\rm crit}, \tau_{\rm crit})$, and terminating at the saturation point $(\rho_0, 0)$ (dashed curve). The points on this boundary can be obtained from fig. 3 by means of a Maxwell construction. Inside the coexistence region, the spinodal boundary (solid curve) connects the extrema in the pressure isotherms. Thus it starts at $(\rho_<, 0)$, tops at the critical point, passes through the $(\rho_{\rm lim}, \tau_{\rm lim})$, and terminates at $(\rho_>, 0)$, where $\rho_<$ and $\rho_>$ denote the densities at which the curve $P(\rho, 0)$ has its maximum and minimum, respectively. These characteristic phase points can all easily be determined from the function $P(\rho, \tau)$ shown in fig. 3 and the two boundaries described above can then be approximately delineated. Figure 5 displays the phase diagrams calculated with the von Groote parameter values, using both $\chi = 0$ and the preferred value $\chi = 0.75$. The main effect of switching on the density-dependent term is to shift the critical density towards lower values, from $\rho_{\rm crit} = 0.0681$ fm^{-3} at $\chi = 0$ to $\rho_{\rm crit} = 0.0555$ fm^{-3} at $\chi = 0.75$. The corresponding change in the critical temperature is from $\tau_{\rm crit} = 17.19$ MeV to $\tau_{\rm crit} = 16.66$ MeV. Unfortunately, the experimental determination of the critical point for nuclear matter is still far from possible.

In the phase diagrams in fig. 5, we also delineate the domain within which the pressure is negative (dotted curve). This curve starts near the origin at a small but

finite density (at which the pressure first becomes negative), has its maximum at the point $\rho_{\rm lim}, \tau_{\rm lim}$, and terminates at the saturation point (where the pressure again turns positive). Systems within this phase domain are selfcohesive, since they do not require an external pressure.

3.3 Comparison with microscopic results

It is interesting to compare our results with those of Friedman and Pandharipande [6], who performed a variational calculation of the equation of state based on a realistic Hamiltonian with fitted two and three-nucleon interaction terms. Such calculations are fairly tedious and not easily extended to systems with non-uniform density distributions, whereas the model presented here has been developed specifically for the purpose of treating arbitrary distributions.

Friedman and Pandharipande [6] consider both pure neutron matter and isosymmetric nuclear matter. We can compare our calculations directly with the latter results. First let us consider the effective mass, which in our model is given by $B/m \asymp 1/(1+\bar{\chi}(C/T)4\pi a^3\rho)$. Their effective mass, $m^\star/m$, is plotted versus k_F in fig. 7 of ref. [6]. This quantity has some temperature dependence for densities near saturation, whereas our B/m depends only on the density $\rho \sim k_F^3$. Up to about twice the saturation density the two effective masses agree with each other to within a few percent (our result falls right between their two curves calculated for $\tau = 5$ and $\tau = 20$). However, for higher densities our B falls off more rapidly, so that they differ by a factor of nearly two at $k_F = 3$ fm^{-1}. This difference is undoubtedly a result of the considerable differences in the short-range features of the two models.

Ref. [6] also tabulates the free energy, the pressure, and the entropy for temperatures up to 20 MeV and densities up to 1.8238 fm^{-3}, *i.e.* over ten times the saturation density. The comparison with these quantities can then be made more quantitatively. For the free energy there is agreement to within less than one per cent for densities near saturation. At temperatures above 10 MeV this level of agreement extends down to the lowest density tabulated ($\rho = 0.004323$ fm^{-3}). For low densities and temperatures a significant relative difference develops. This is to be expected because this domain is sensitive to the long-range behavior of the attractive interaction and the two calculations employ quite different values: We use the relatively short range $a = 0.557$ fm (which is determined by fitting to the surface energy), whereas the calculations in ref. [6] are made with a range of $1/0.7 \approx 1.43$ fm (according to ref. [9]), the range of the one-pion exchange force. Therefore, our model probably underestimates the binding for very dilute uniform distributions. In the other extreme, for supersaturation densities, the short-range properties are important. With our chosen parameter values, we have a compressibility modulus of $K = 304.5$ MeV, whereas the corresponding value for the microscopic model is 240 MeV. Consequently, one should expect our results to significantly exceed the microscopic values in the high-density domain. This is also brought out and at ten times normal density our results exceed those of ref. [6] by nearly 80%. (At this high density the temperature dependence is insignificant, in the range considered.)

For the entropy the two calculations agree to within a few per cent, for densities

up to 2-3 times normal. At higher densities the difference grows steadily larger and at ten times normal the entropy of ref. [6] is nearly twice ours, relatively independently of temperature. This difference is most likely due to the aforementioned difference in effective mass at these high densities.

Finally let us compare the results for the pressure. In the domain of low density and high temperature the two calculations again agree to within a few per cent. However, as we move away from this vapor-like scenario, significant differences emerge and at ten times normal density our pressure exceeds that of ref. [6] by nearly 70% (nearly independently of temperature). This kind of behavior is to be expected from the results discussed above. In spite of this difference, the associated phase diagrams are fairly similar. For example, with our preferred parameter values we obtain a critical temperature of $\tau_{\rm crit} = 16.66$ MeV, while ref. [6] reports 17.5 ± 1 MeV. It should be added that if substantially different χ values are employed then our results would deviate significantly more from those of ref. [6].

This detailed comparison with an often-cited microscopic calculation serves to illustrate what can be expected from our model. Since the two models differ with respect to such characteristic quantities as interaction range and compressibility modulus, they should not be expected to yield identical results. By adjusting these quantities the two calculations can, presumably, be brought into better mutual agreement, should that be deemed desirable. However, the overall reasonable behavior of the calculated results suggests that our model, though relatively simple, may be quantitatively useful for addressing general nuclear density distributions.

4 Statistical distributions

An important advantage of the present formulation is that it is not restricted to equilibrium configurations but provides the statistical weight for arbitrary density distributions. Thus statistical fluctuations can be directly studied. To illustrate this feature, let us consider the statistical weight of the uniform system as a function of its density, for a specified temperature. For this purpose, it is convenient to consider the quantity $\omega = (1/A)\ln W = \sigma - \beta\epsilon$, which is the logarithm of the statistical weight $W[\rho]$ divided by the number of nucleons in the system, A. [For infinite matter the free energy diverges in proportion to A and the statistical weight becomes a singular distribution sharply peaked at the most probable configuration. However, for finite systems it is possible to make excursions away from equilibrium. Such systems can be studied by imposing periodic boundary conditions.] The quantity ω is shown in fig. 6. For low temperatures the statistical weight is peaked near the saturation density, as expected, and the most favored density shifts gradually towards more dilute values as the temperature is raised. In concert with this shift, the peak broadens and the vapor spike in the dilute region near zero density grows increasingly prominent. Thus, the system is in principle metastable, in accordance with the fact that a nucleus held at a constant temperature will gradually disassemble into a dilute gas through sequential evaporation. When the temperature reaches the value $\tau_{\rm lim}$, there is no longer a maximum at finite density and the statistical weight increases monotonically

with decreasing density, basically reflecting the increase of the entropy with volume. This *limiting temperature* is thus the highest one for which a self-cohesive metastable nucleus can exist. Above this limit, in the range $\tau_{\rm lim} < \tau < \tau_{\rm crit}$ metastability can only be maintained if an external pressure is provided.

4.1 Density ripples

On the basis of the statistical weight, as illustrated in fig. 6, it is straightforward to calculate the amount of density fluctuation in a given finite system. Fig. 6 illustrates the applicability of the model to the statistical distribution of densities for uniform systems. It is of considerable interest to explore also non-uniform densities. This is particularly important in the region of negative pressure where the system prefers to phase separate so as to exploit the cohesion of nuclear matter. It is especially instructive to consider density distortions of harmonic form,

$$\rho(\mathbf{r}) \;=\; \bar{\rho}\,(1 + c\cos\mathbf{k}\cdot\mathbf{r})\;, \tag{30}$$

where $\mathbf{k}$ is the specified wave vector and c the amplitude of the undulation. The corresponding auxiliary function can then be readily obtained analytically as an elementary Fourier transform,

$$\mathcal{R}(\mathbf{r}) = 4\pi a^3\bar{\rho}\,(1 + c\,\frac{\cos\mathbf{k}\cdot\mathbf{r}}{1+a^2k^2})\;. \tag{31}$$

The response of uniform nuclear matter to such harmonic ripples can be addressed analytically, provided the amplitudes are sufficiently small to render the response linear. The average free energy per particle is then of the form

$$\phi = \int d\mathbf{r} f(\mathbf{r}) / \int d\mathbf{r}\rho(\mathbf{r}) = \underline{\phi} + \frac{1}{2}c^2\phi_2\;, \tag{32}$$

where $f(\mathbf{r}) = e(\mathbf{r}) - \tau s(r)$ is the free-energy density, and $\underline{\phi} = \underline{\epsilon} - \tau\underline{\sigma}$ is the free energy per particle when the amplitude c vanishes so the system is uniform. The restoring coefficient ϕ_2 can be obtained by averaging the second-order terms in $f(\mathbf{r})$. The resulting expression is somewhat complicated. However, for zero temperature we have $\kappa = \tilde{\kappa}$ and the formula for ϕ_2 is then relatively simple,

$$\phi_2^{\tau=0} = \frac{1}{3}T_F(\frac{\bar{\rho}}{\rho_0})^{2/3}(1 + 4\pi a^3\bar{\rho}\frac{C}{T}) - \frac{2\pi a^3\bar{\rho}C}{1+a^2k^2}(1 - 2\frac{T_F}{T})\;, \tag{33}$$

where ρ_0 denotes the saturation density, as usual. The restoring coefficient ϕ_2 is a steadily decreasing function of the wavelength of the ripples, $\lambda = 2\pi/k$. Whenever it is negative, the system is unstable against infinitesimal oscillations of the specified wavelength. Outside the phase coexistence region, the uniform system is generally stable against undulations of any wavelength and amplitude. Inside the spinodal boundary, the system is stable against distortions of small wavelength $\lambda < \lambda_{\rm max}$, but turns unstable against undulations with a sufficiently long wavelength $\lambda > \lambda_{\rm max}$. In

the intermediate region the system is metastable: it is stable with respect to harmonic undulations, but there exist finite redistributions of the matter that have a more favorable statistical weight. (For example, cold uniform matter slightly below saturation prefers to condense into large separated regions of matter at normal density.) The calculated values of λ_{max} inside the spinodal boundary are shown in fig. 7 (open circles) as functions of the temperature τ, for a few selected values of the mean density $\bar{\rho}$.

The above results pertain to infinitesimal deviations from uniformity, for which first-order perturbation theory can be used. However, it is also of interest to explore the behavior of the system when distortions of finite size are induced, especially in the intermediate region where the stability of the system depends on the amplitude of the distortion. Since $\kappa(\mathbf{r})$ depends on $\rho(\mathbf{r})$ in a non-linear fashion, the induced undulation of $\kappa(\mathbf{r})$ is not harmonic and and so the finite-amplitude response must be obtained numerically. This can be accomplished quickly and accurately with our model, utilizing the method described in Appendix A. The auxiliary function $\mathcal{K}_{\mathrm{eff}}(\mathbf{r})$ must then be calculated by performing the convolution explicitly. An efficient method for this task is described in Appendix B.

We have examined the response of uniform matter to periodic ripples of finite amplitude. For given values of the temperature τ and the mean density ρ, the free energy F (and hence the statistical weight W) can be considered as a function of the wavelength $\lambda = 2\pi/k$ and the amplitude c of the undulation imposed. If the statistical weight decreases when the amplitude c is increased from zero, the system is considered stable against the perturbation, and otherwise it is unstable.

In fig. 7 we show the calculated values of the maximum wavelength at which the system looses stability, λ_{max}. These results have been obtained by comparing the statistical weight corresponding to the small finite amplitude of $c = 0.1$ with that of the uniform system (for which c vanishes). We note that the values for λ_{max} obtained in this manner deviate little from those associated with infinitesimal distortions, as would be expected.

Curiously, it may happen that the statistical weight first increases with the amplitude c, but then exhibits a maximum and ultimately falls off. This behavior is indicative of spontaneous symmetry breaking. Thus, if prepared with a uniform density and *only* allowed to explore undulations of the particular wavelength, the system would stabilize with a distribution having finite-amplitude ripples. Of course, this configuration would be unstable against more general redistributions, so this feature has little practical import.

We also see from fig. 7 that as the temperature is raised the loss of stability occurs at an ever longer wave length, as expected from the above general remarks, since the system then moves closer to the coexistence boundary outside which it is fully stable. We also note that the resulting values of λ_{max} depend significantly on the value of the parameter χ. This feature may affect the quantitative predictions for nuclear multifragmentation phenomena. It may also be used to ascertain the validity of the commonly taken approach in which the fragmenting system is assumed to appear as a collection of distinct (though possibly interacting) fragments (that may be immersed in a nucleon vapor), see refs. [10, 11, 12], for example.

It should be added, that the significance of instabilities in a given dynamical process depends on the rate at which the unstable modes develop. This is especially important in nuclear collisions where the time scales are very short. The initial growth rate of harmonic density ripples has been studied by Heiselberg *et al.*[13].

5 Summary and outlook

In the laboratory, a large variety of physical environments can be created transiently by means of nuclear reactions at intermediate energies. The interpretation of such collision experiments, which are often aimed at probing the nuclear equation of state, depends critically on our understanding of the statistical properties of non-uniform nuclear matter at finite temperature. We have presented a model that can be brought to bear on these problems. The model may also prove of some utility in connection with the supernova process, in which matter is compressed to densities near the saturation value and the temperature reaches several to many MeV, although we are not presently contemplating astrophysical applications.

In this first presentation of the model, we have derived the central formalism, including expressions for the statistical weight and the pressure. We have considered two families of interactions, corresponding to two different sets of fitted values of the Seyler-Blanchard parameters, and each parametrized by the quantity χ governing the strength of the new density-dependent term (and thereby determines the energy dependence of the optical potential). We have found that while there is little sensitivity to the specific Seyler-Blanchard parameters used, the statistical properties do depend significantly on the value of χ. Even so, the limiting temperature $\tau_{\rm lim}$ happens to be nearly the same for $\chi = 0$ (the pure Seyler-Blanchard interaction having $B \approx 0.38m$) and for the realistic value $\chi = 0.75$ (giving $B \approx 0.71m$).

The capability of the model to treat non-uniform systems was illustrated by considering the response of matter to ripples of finite amplitude. It was found that the maximum wavelength for which the system is stable, $\lambda_{\rm max}$, depends significantly on the value of χ. This finding may be especially important for studies of nuclear multifragmentation, since the transformation of the system into an assembly of (pre)fragments may well be strongly influenced by such instabilities.

The developed model gives a consistent statistical description of nuclear systems with arbitrary density distributions, within the confines of semi-classical mean-field theory. The model combines three important features: 1) it is conceptually simple and computationally relatively easy; 2) it has a rather general applicability, namely to arbitrary density distributions held at a fixed temperature; and 3) it agrees quantitatively with general (average) nuclear properties, both as regards a broad spectrum of experimental data (binding, optical potential, *etc.*) and with respect to theoretical expectations based on more elaborate calculations (such as those reported in ref. [6]).

As already mentioned, the purpose of the present paper is to present the key parts of the model, including certain useful technical tools. Accordingly, we have included only a few instructive applications. We foresee several further developments and applications of the approach. One direction of development is the extension of the

numerical treatment to two and three dimensions and the inclusion of the Coulomb force. Though mostly technical in nature, these elaborations are needed to make more direct contact with experiment. Another development is the inclusion of collective flow in the formulation. This formal extension can readily be made on the basis of ref. [8] and it will broaden the scope of the model to more dynamical scenarios. This is particularly important in the context of nuclear multifragmentation, where the individual fragments may carry an overall momentum (both statistical and collective) and so the system cannot be properly described within the confines of static theory. Finally, the model is developed with a view towards performing direct statistical sampling of the density distributions $\rho(\mathbf{r})$, by a suitable Metropolis-type method utilizing the statistical weight $W[\rho]$. This will make it possible to study the statistical properties of the system in situations where the fluctuations are large. Thus the model may help elucidate a variety of aspects related to the physical properties of hot nuclear systems away from equilibrium. We are presently pursuing these aspects.

This work was supported in part by the Director, Office of Energy Research, Division of Nuclear Physics of the Office of High Energy and Nuclear Physics of the U.S. Department of Energy under Contract No. DE-AC03-76SF00098. We also wish to acknowledge useful discussions with W.D. Myers and W.J. Swiatecki. On of us (ELM) would like to express his gratitude to the Nuclear Theory Group at the LBL for the kind hospitality.

A Fermi-Dirac moments

For any power $n > -1$ we may define the following Fermi-Dirac moments

$$F_n(\alpha) = \int_0^\infty dx \, \frac{x^n}{1+\exp(x-\alpha)} , \tag{A.1}$$

$$G_n(\alpha) = \int_0^\infty dx \, x^n \left[\frac{\ln(1+\mathrm{e}^{x-\alpha})}{1+\mathrm{e}^{x-\alpha}} + \frac{\ln(1+\mathrm{e}^{\alpha-x})}{1+\mathrm{e}^{\alpha-x}} \right] , \tag{A.2}$$

where the modulation factor in the integrand for F_n is the Fermi-Dirac occupancy coefficient $f = 1/(1+\exp(x-\alpha))$ and the one in the integrand for G_n is the combination $f \ln f + \bar{f} \ln \bar{f}$ entering in the entropy expression. These dimensionless quantities are useful, because certain key quantities can be expressed in terms of them. For example, we have $\rho \sim F_{1/2}(\alpha)$, $\kappa \sim F_{3/2}(\alpha)$, and $s \sim G_{1/2}(\alpha)$.

When calculating the variations $\delta\kappa/\delta\rho$ and $\delta s/\delta\rho$ (see eqs. (27) and (28)), we need to also evaluate momentum integrals peaked in the Fermi surface. These can be expressed in terms of the associated Fermi-Dirac moments

$$F_n'(\alpha) = \frac{\partial}{\partial\alpha} F_n(\alpha) = \int_0^\infty dx \, x^n f\bar{f} = nF_{n-1}(\alpha) , \tag{A.3}$$

$$G_n'(\alpha) = \frac{\partial}{\partial\alpha} G_n(\alpha) = \int_0^\infty dx \, x^n f\bar{f}(\ln\bar{f} - \ln f) = nG_{n-1}(\alpha) . \tag{A.4}$$

The modulation factor $f\bar{f}$ (where $\bar{f} = 1 - f$ is the Fermi-Dirac availability) acts to concentrate the integrand around the Fermi surface. The relations on the far right relate the primed moments to the unprimed ones; this convenient feature reduces the number of moments needed.

Moreover, it is elementary to prove the following relation

$$G'_n(\alpha) = (n+1)F_n(\alpha) - \alpha n F_{n-1}(\alpha) \ , \tag{A.5}$$

so that the G moments can be related directly to the F moments,

$$G_n(\alpha) = \frac{n+2}{n+1} F_{n+1}(\alpha) - \alpha F_n(\alpha) \ . \tag{A.6}$$

Therefore, the only Fermi-Dirac moments needed are F_n for the three powers $n = -\frac{1}{2}, \frac{1}{2}, \frac{3}{2}$. These can be calculated and tabulated ahead of time, thus reducing the computational problem considerably.

In the actual applications, the quantity $\xi = \rho/\rho_\tau$ is given, and the fugacity α must be determined as the solution to the relation $\xi = F_{1/2}(\alpha)$. Subsequently, the moments $F_{3/2}$ and $F_{-1/2}$ can be calculated. Thus, we need the two functions

$$\tilde{F}_{\frac{3}{2}}(\xi) = F_{\frac{3}{2}}(F^{-1}_{\frac{1}{2}}(\xi)) \ , \ \tilde{F}_{-\frac{1}{2}}(\xi) = F_{-\frac{1}{2}}(F^{-1}_{\frac{1}{2}}(\xi)) \ , \tag{A.7}$$

These universal dimensionless functions can be evaluated numerically and tabulated once and for all, which leads to a considerable savings in computational effort. These functions are defined in the interval $0 \leq \xi \leq \infty$. In the domains of very small or very large values of the argument ξ, use can be made of simple analytical approximations, thus reducing the amount of tabular storage space needed. These two limits are described below.

For sufficiently high temperatures τ, or sufficiently low densities ρ, we have $\xi \to 0$ and so the fugacity α decreases without bound. and the *classical* limit is approached. The exponential in the denominator of F then tends to infinity and a quickly converging expansion can be made,

$$F_n^{\text{classical}}(\alpha) = \Gamma(n+1)\ \mathrm{e}^{\alpha} \sum_{k \geq 0} \frac{(-)^k}{(k+1)^{n+1}}\ \mathrm{e}^{k\alpha} \ . \tag{A.8}$$

From the relationship $\xi = F_{\frac{1}{2}}(\alpha)$ we then find, to second order in ξ,

$$\begin{aligned} \alpha &= F^{-1}_{\frac{1}{2}}(\xi) \approx \ln \frac{2\sqrt{2}\xi}{\sqrt{2\pi} - \xi} \ , \\ \tilde{F}_{\frac{3}{2}}(\xi) &= F_{\frac{3}{2}}(\alpha(\xi)) \approx \frac{3}{2}\xi\ \frac{\sqrt{2\pi} - \frac{1}{2}\xi}{\sqrt{2\pi} - \xi} \ , \qquad \text{(A.9)} \\ \tilde{F}_{-\frac{1}{2}}(\xi) &= F_{-\frac{1}{2}}(\alpha(\xi)) \approx 2\xi\ \frac{\sqrt{2\pi} - 2\xi}{\sqrt{2\pi} - \xi} \ . \qquad \text{(A.10)} \end{aligned}$$

The above expressions are used for $\xi < 0.01$, leading to an accuracy of better than 0.01%.

In the opposite extreme, low temperatures or high densities, we have $\xi \to \infty$ and so α increases without bound. This is the *quantal* limit and we may then employ the Sommerfeld expansion [14] and obtain

$$F_n^{\text{quantal}}(\alpha) \approx \theta(-\alpha) - \frac{\pi^2}{6}\frac{(n+1)n}{\alpha^2} - \frac{7\pi^4}{360}\frac{(n+1)n(n-1)(n-2)}{\alpha^4} , \tag{A.11}$$

where $\theta(x)$ is the truncation function. Using this result for $n = \frac{1}{2}$ we find

$$\alpha \approx \alpha_0 \left[1 - \frac{1}{12}(\frac{\pi}{\alpha_0})^2 - \frac{1}{80}(\frac{\pi}{\alpha_0})^4\right] , \tag{A.12}$$

where $\alpha_0 = (\frac{3}{2}\xi)^{2/3}$. The two universal functions are then given as

$$\tilde{F}_{\frac{3}{2}}(\xi) \approx \frac{2}{5}\alpha_0^{\frac{5}{2}} \left[1 + \frac{5}{12}(\frac{\pi}{\alpha_0})^2 - \frac{1}{16}(\frac{\pi}{\alpha_0})^4\right] , \tag{A.13}$$

$$\tilde{F}_{-\frac{1}{2}}(\xi) \approx 2\alpha_0^{\frac{1}{2}} \left[1 + \frac{1}{12}(\frac{\pi}{\alpha_0})^2 - \frac{11}{360}(\frac{\pi}{\alpha_0})^4\right] . \tag{A.14}$$

The above expressions are used for $\xi > 100$. For $\xi = 100$ they are accurate to within 0.01%.

The utility of the Fermi-Dirac moments for thermodynamic studies of fermion systems was recognized already by Stoner [15] and our above exposition is in accordance with his results. These moments were also employed in the work by Küpper *et al.* [3].

B Convolution

We here describe an efficient method for performing a convolution with a Yukawa function in a semi-infinite geometry. This method was developed in connection with the work reported in [8], but not published at the time. We have since found it to be useful in a variety of contexts and therefore wish to make it generally available by including a brief description here.

We consider a semi-infinite geometry, *i.e.* we consider a system that has translational invariance in two of the three spatial dimensions. The physical quantities then vary in only one direction, the x direction, say. The general task is to perform the convolution

$$\mathcal{F}(\mathbf{r}_1) \;=\; \int d\mathbf{r}_2 \, \frac{\mathrm{e}^{-r_{12}/a}}{r_{12}/a} \, f(\mathbf{r}_2) \;=\; 2\pi a^2 \int dx_2 \, \mathrm{e}^{-|x_{12}|/a} \, f(x_2) \; . \tag{B.1}$$

Here the given function $f(\mathbf{r})$ depends only on x because of the translational invariance in the yz plane, and the Yukawa function can then be integrated over $\boldsymbol{\rho} = (y, z)$, leaving an exponential. [This result is readily obtained by using cylindrical coordinates and exploiting the fact that $rdr = \rho d\rho$.]

The first step is to split the integral into two,

$$\mathcal{F}(x_1) = 2\pi a^2 \int_{-\infty}^{x_1} dx_2 \, \mathrm{e}^{(x_2-x_1)/a} f(x_2) + 2\pi a^2 \int_{x_1}^{\infty} dx_2 \, \mathrm{e}^{(x_1-x_2)/a} f(x_2) \;=\; \mathcal{F}^-(x_1) + \mathcal{F}^+(x_1) \; . \tag{B.2}$$

It is then possible to derive the following recursion relations for the values of $\mathcal{F}^-$ and $\mathcal{F}^+$ at neighboring grid points,

$$\mathcal{F}^-(x_1+\Delta) = \mathcal{F}^-(x_1)\,\mathrm{e}^{-\Delta/a} + 2\pi a^2 \int_{x_1}^{x_1+\Delta} dx_2\, \mathrm{e}^{(x_2-x_1-\Delta)/a} f(x_2)\ , \quad \text{(B.3)}$$

$$\mathcal{F}^+(x_1-\Delta) = \mathcal{F}^+(x_1)\,\mathrm{e}^{-\Delta/a} + 2\pi a^2 \int_{x_1-\Delta}^{x_1} dx_2\, \mathrm{e}^{(x_1-\Delta-x_2)/a} f(x_2)\ . \quad \text{(B.4)}$$

B.1 Generalized trapezoidal integration

In order to permit a fast evaluation of the integrals over the small intervals of size Δ, a simple two-point formula has been developed. It is designed to yield the exact result when the function $f(x)$ is locally linear. It is elementary to show that if $f(x)$ is a second-order polynomial, then the requirement

$$\int_{-\Delta/2}^{\Delta/2} dx\, \mathrm{e}^{x/a} f(x) = w_- f(-\frac{\Delta}{2}) + w_+ f(\frac{\Delta}{2})\ , \quad \text{(B.5)}$$

yields the expressions

$$w_\pm = \Delta\, \mathrm{e}^{\pm\Delta/2a} \left[\mathrm{e}^{\mp\Delta/a} - 1 \pm \frac{\Delta}{a}\right] (\frac{a}{\Delta})^2 \quad \text{(B.6)}$$

for the integration weights. [It is easy to verify that $w_- + w_+ \approx \Delta$ and $w_\pm \approx \Delta/2$ when $\Delta \ll a$.]

By proceeding in the same manner, it is possible to also derive a generalization of Simpson's three-point integration formula. The result is

$$\int_{-\Delta}^{\Delta} dx\, \mathrm{e}^{x/a} f(x) = w_- f(-\Delta) + w_0 f(0) + w_+ f(\Delta)\ , \quad \text{(B.7)}$$

with the weights

$$\begin{aligned} w_- &= \frac{a^3}{2\Delta^2}\left[\left(2-\frac{\Delta}{a}\right)\mathrm{e}^{\Delta/a} - \left(2+3\frac{\Delta}{a}+2(\frac{\Delta}{a})^2\right)\mathrm{e}^{-\Delta/a}\right]\ , \\ w_0 &= \frac{2a^3}{\Delta^2}\left[(\Delta-a)\mathrm{e}^{\Delta/a} + (\Delta+a)\mathrm{e}^{-\Delta/a}\right]\ , \\ w_+ &= \frac{a^3}{2\Delta^2}\left[\left(2-3\frac{\Delta}{a}+2(\frac{\Delta}{a})^2\right)\mathrm{e}^{\Delta/a} - (2+\frac{\Delta}{a})\mathrm{e}^{-\Delta/a}\right]\ . \end{aligned} \quad \text{(B.8)}$$

Note that the usual Simpson weights are recovered when $\Delta \ll a$, $w_- \approx w_+ \approx \Delta/3$ and $w_0 \approx 4\Delta/3$.

B.2 Specific application

Assume that the function $f(x)$ is given on N equidistant grid points with separation Δ and we need to evaluate the result of the convolution at the same points. This can be quickly accomplished by using the recursion formulas (B.3) and (B.4), once the starting values $\mathcal{F}_1^-$ and $\mathcal{F}_N^+$ have been calculated.

In the context where the method was originally developed [8], the functions were constant outside of the explicitly considered domain, and hence it was trivial to obtain the starting values $\mathcal{F}_1^-$ and $\mathcal{F}_N^+$. In the present context we have periodic boundary conditions, and these values must then be calculated by explicit numerical integration. Using the above simple two-point formula, we find

$$\mathcal{F}_1^- = 2\pi a^2 \mathrm{e}^{\Delta/2a} \left[w_- \mathrm{e}^{-\Delta/a} f_1 + \bar{w}\, \mathrm{e}^{-\Delta/a} \left(f_N + \mathrm{e}^{-\Delta/a} (f_{N-1} + \cdots) \right) \right] , \quad \text{(B.9)}$$

$$\mathcal{F}_N^+ = 2\pi a^2 \mathrm{e}^{\Delta/2a} \left[w_- \mathrm{e}^{-\Delta/a} f_N + \bar{w}\, \mathrm{e}^{-\Delta/a} \left(f_1 + \mathrm{e}^{-\Delta/a} (f_2 + \cdots) \right) \right] , \quad \text{(B.10)}$$

where $\bar{w} = w_+ + w_- / \exp(\Delta/a)$. The remaining values are then obtained using (B.3) and (B.4),

$$\mathcal{F}_{n+1}^- = \mathcal{F}_n^-\, \mathrm{e}^{-\Delta/a} + 2\pi a^2 (w_- f_n + w_+ f_{n+1})\, \mathrm{e}^{-\Delta/2a} , \quad \text{(B.11)}$$

$$\mathcal{F}_{n-1}^+ = \mathcal{F}_n^+\, \mathrm{e}^{-\Delta/a} + 2\pi a^2 (w_+ f_{n-1} + w_- f_n)\, \mathrm{e}^{-\Delta/2a} . \quad \text{(B.12)}$$

The computational advantage of this method is that only two sweeps through the grid are required, one upwards to obtain $\mathcal{F}^-$ and one downwards to obtain $\mathcal{F}^+$, in contradistinction with the N sweeps required by general methods (one sweep for each calculated value of $\mathcal{F}$). This gives a significant improvement in efficiency.

References

[1] W.D. Myers and W.J. Swiatecki, Ann. Phys. **55** (1969) 395

[2] R.G. Seyler and C.H. Blanchard, Phys. Rev. **124** (1961) 227; **131** (1963) 355

[3] W.A. Küpper, G. Wegman, and E.R. Hilf, Ann. Phys. **88** (1974) 454

[4] W.D. Myers and W.J. Swiatecki, LBL-28693 (1990), Ann. Phys. (in press)

[5] J.M. Lattimer and D.G. Ravenhall, Ap. J. **223** (1978) 314

[6] B. Friedman and V.R. Pandharipande, Nucl. Phys. **A361** (1981) 502

[7] H. von Groote, Proc. 3rd Int. Conf. on Nuclei Far From Stability, ed. R. Klapish, CERN 76-13 (1976) 595

[8] J. Randrup, Nucl. Phys. **A259** (1976) 253

[9] I.E. Lagaris and V.R. Pandharipande, Nucl. Phys. **A359** (1981) 349

[10] S.E. Koonin and J. Randrup, Nucl. Phys. **A474** (1987) 173

[11] G. Fai and J. Randrup, Nucl. Phys. **A487** (1988) 397

[12] J.A. López and J. Randrup, Nucl. Phys. **A503** (1989) 183

[13] H. Heiselberg, C.J. Pethick, and D.G. Ravenhall, Phys. Rev. Lett. **61** (1988) 818

[14] S. Chandrasekhar, *Stellar Structure*, Dover Publications, Inc., 1957, p. 389

[15] E.C. Stoner, Phil. Mag. **28** (1939) 257

Figure 1: Specific energy

The energy per nucleon $\epsilon = E/A$ in uniform isosymmetric nuclear matter as a function of the nucleon density ρ, for a range of imposed temperatures, $\tau = 0, 5, 10, 15, 20$ MeV. Results are also shown for the limiting temperature $\tau_{\rm lim} = 13$ MeV at which nuclear matter ceases to be self-cohesive. Both results with the standard Seyler-Blanchard interaction (1) and the generalized one (15) are shown, for the von Groote set of parameter values.

Figure 2: Specific entropy

For the same two models as in fig. 1, the entropy per nucleon $\sigma = S/A$ is shown as a function of the nucleon density ρ, and for the same temperatures τ. (Since the entropy vanishes for zero temperature, the $\tau = 0$ curve is absent.)

Figure 3: Equation of state

Similarly to figs. 1 and 2, the pressure P in uniform isosymmetric nuclear matter is displayed as a function of the nucleon density ρ, for a range of temperatures τ.

Figure 4: Characteristic phase properties

The limiting temperature $\tau_{\rm lim}$ (above which the pressure is never negative) and the corresponding density $\rho_{\rm lim}$ as functions of the parameter χ, as well as the values $\tau_{\rm crit}$ and $\rho_{\rm crit}$ associated with the critical point where the liquid and vapor phases coalesce. The solid curves refer to the parameters fitted by von Groote [7], while the dashed curves are obtained with the original Myers-Swiatecki values [1]. (The displayed density values have a numerical uncertainty of around 0.002 fm^{-3}, whereas the temperatures are quite accurate.)

Figure 5: Phase diagram

The phase diagram for symmetric nuclear matter in the $\rho - \tau$ plane, as calculated with the von Groote parameter values for $\chi = 0$ and $\chi = 0.75$. The critical point is shown by the solid dot. The solid curve is the spinodal line, inside which the system is mechanically unstable. The dashed curve delineates the region inside which the vapor and liquid phases may coexist in thermodynamic and mechanical equilibrium. Uniform matter is metastable between these two boundaries. Moreover, the dotted curve encloses the selfcohesive domain in which the pressure is negative.

Figure 6: Statistical weight

As a function of the density ρ and for a range of temperatures τ is shown the reduced quantity $\omega = (1/A) \ln W = -\beta\phi = \sigma - \beta\epsilon$, which is equal to minus the free energy per nucleon divided by the temperature. Because it is thus independent of the actual size of the system, this display can be regarded as a universal representation of the statistical weight.

Figure 7: Critical wavelength

The maximum wavelength $\lambda_{\max}$, for which a hot uniform system inside the spinodal boundary is stable against harmonic density undulations (see eq. (30)), as a function of the temperature τ, for three selected values of the average nucleon density $\bar{\rho}$. The open circles show the results in the limit of infinitesimal amplitudes, while the curves were obtained with the finite amplitude $c = 0.1$.

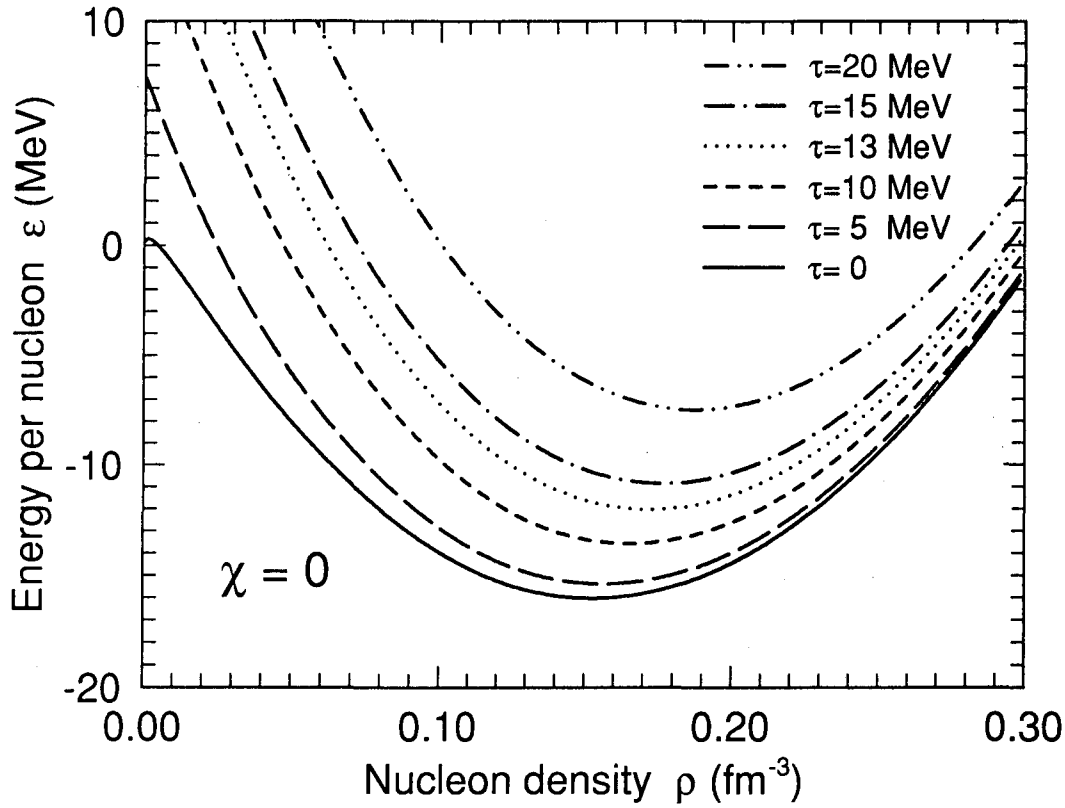
10
0
-10
-20
0.00
0.10
0.20
0.30
Energy per nucleon ε (MeV)
Nucleon density ρ (fm^{-3})
τ=20 MeV
τ=15 MeV
τ=13 MeV
τ=10 MeV
τ= 5 MeV
τ= 0
χ = 0

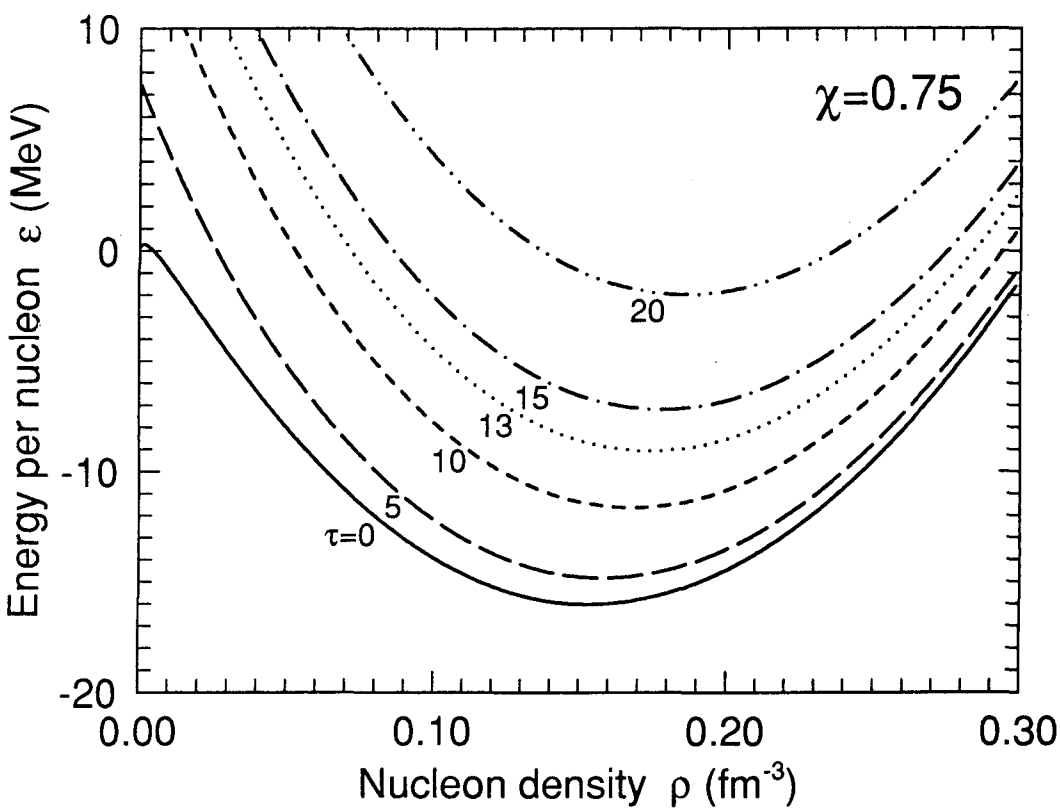
10
0
-10
-20
0.00
0.10
0.20
0.30
Energy per nucleon ε (MeV)
Nucleon density ρ (fm^{-3})
χ=0.75
20
15
13
10
5
τ=0

Figure 1

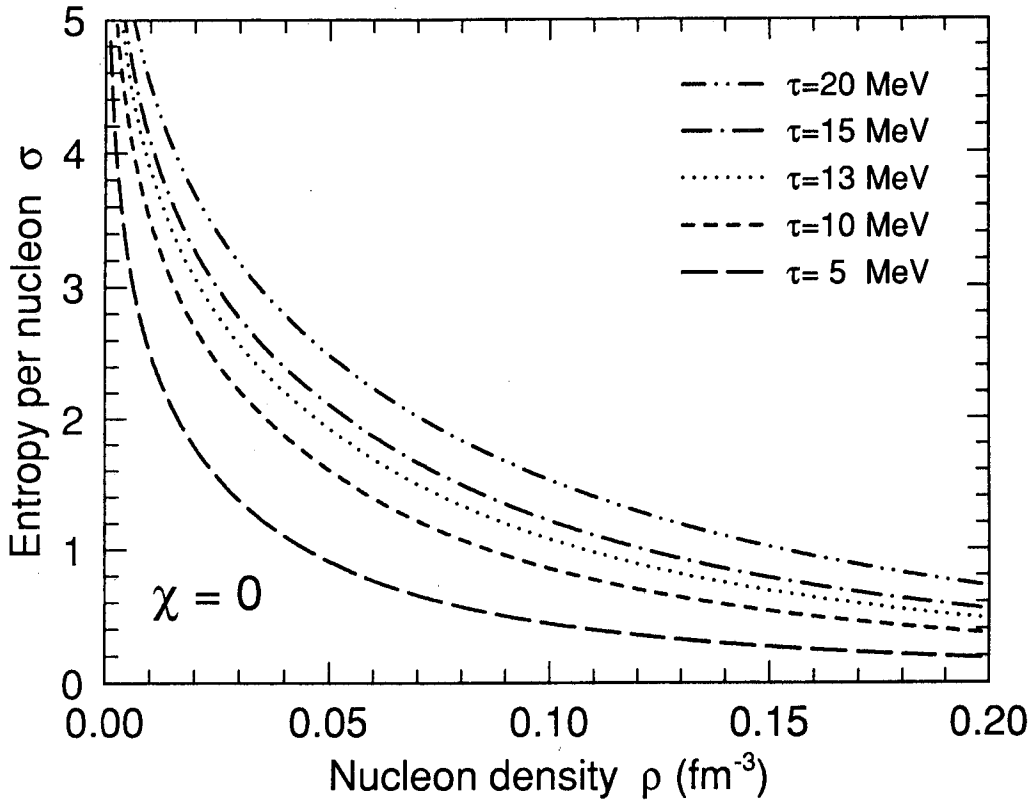
τ=20 MeV
τ=15 MeV
τ=13 MeV
τ=10 MeV
τ= 5 MeV
χ = 0
Entropy per nucleon σ
Nucleon density ρ (fm^{-3})
0
1
2
3
4
5
0.00
0.05
0.10
0.15
0.20

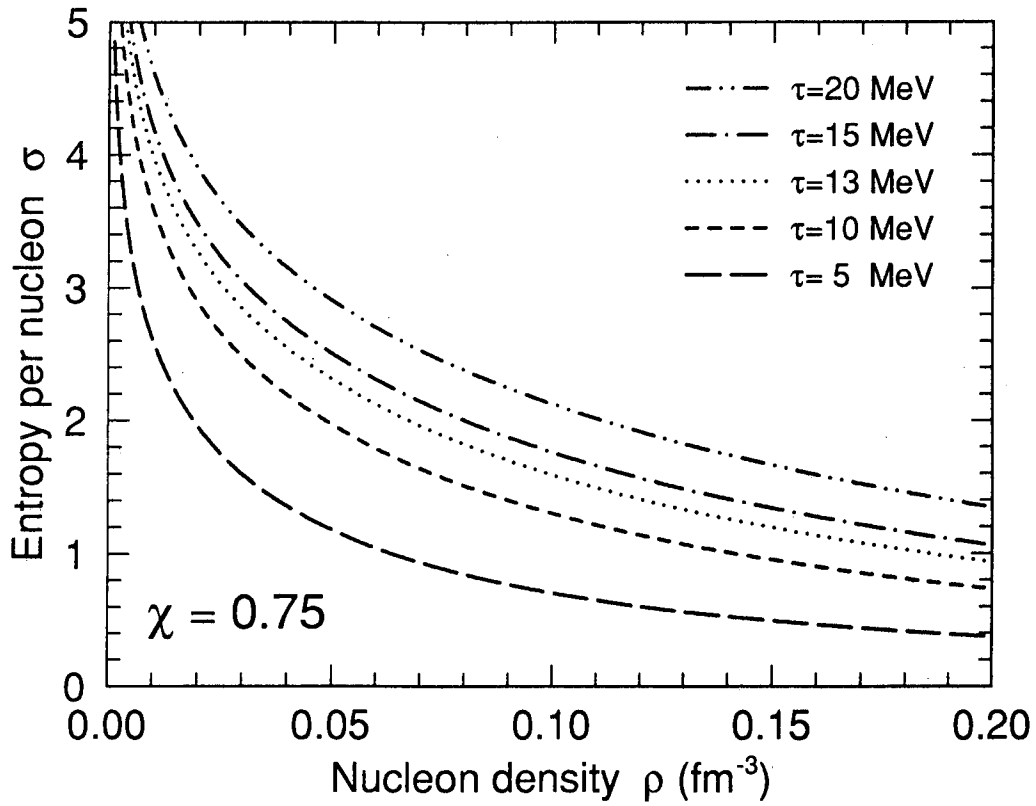
τ=20 MeV
τ=15 MeV
τ=13 MeV
τ=10 MeV
τ= 5 MeV
χ = 0.75
Entropy per nucleon σ
Nucleon density ρ (fm^{-3})
0
1
2
3
4
5
0.00
0.05
0.10
0.15
0.20

Figure 2

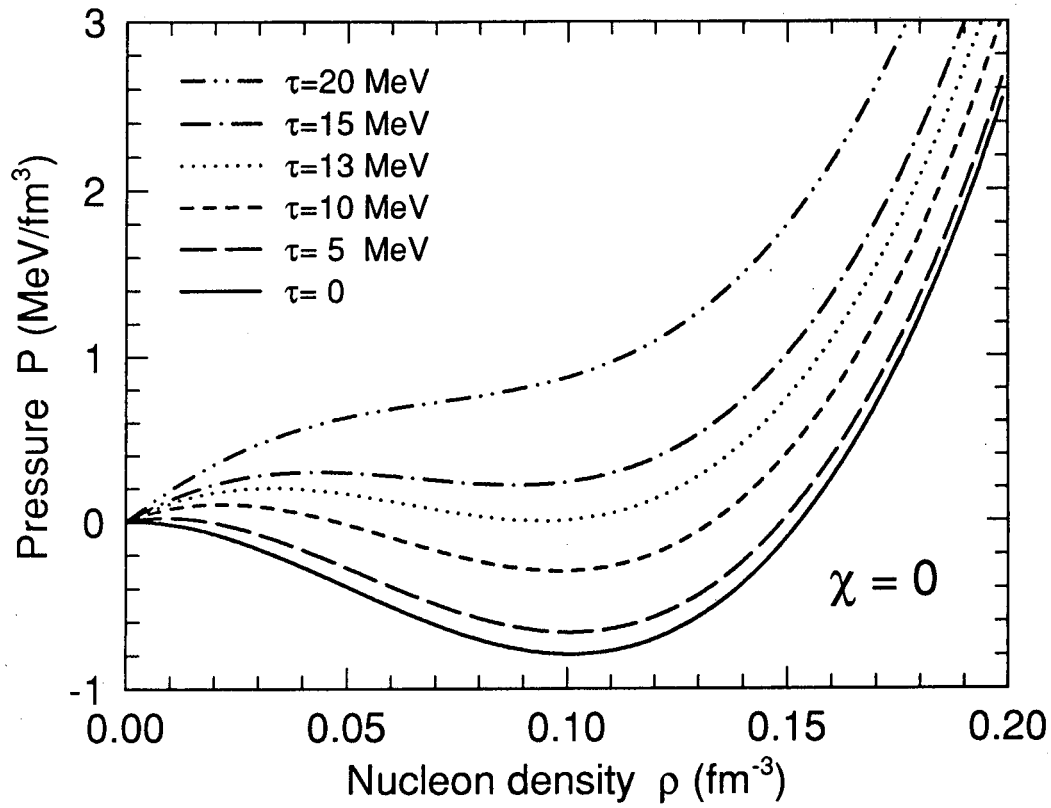
τ=20 MeV
τ=15 MeV
τ=13 MeV
τ=10 MeV
τ= 5 MeV
τ= 0
χ = 0
Pressure P (MeV/fm³)
Nucleon density ρ (fm⁻³)
3
2
1
0
-1
0.00
0.05
0.10
0.15
0.20

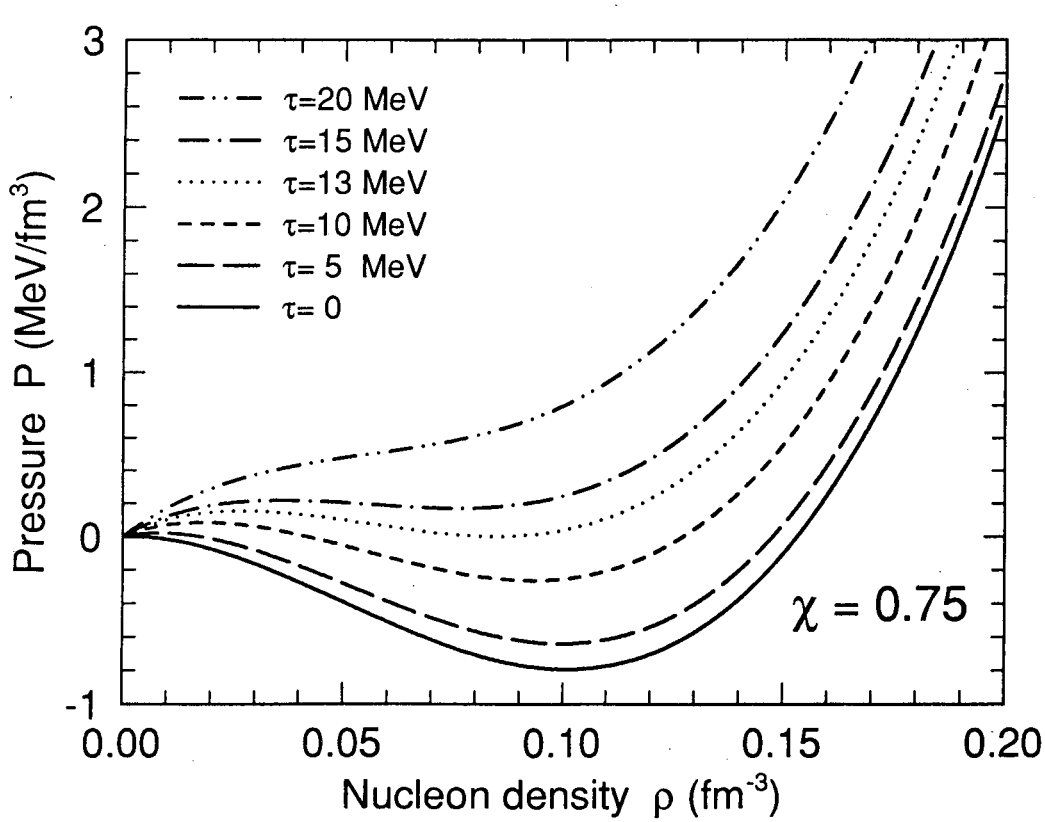
τ=20 MeV
τ=15 MeV
τ=13 MeV
τ=10 MeV
τ= 5 MeV
τ= 0
χ = 0.75
Pressure P (MeV/fm³)
Nucleon density ρ (fm⁻³)
3
2
1
0
-1
0.00
0.05
0.10
0.15
0.20

Figure 3

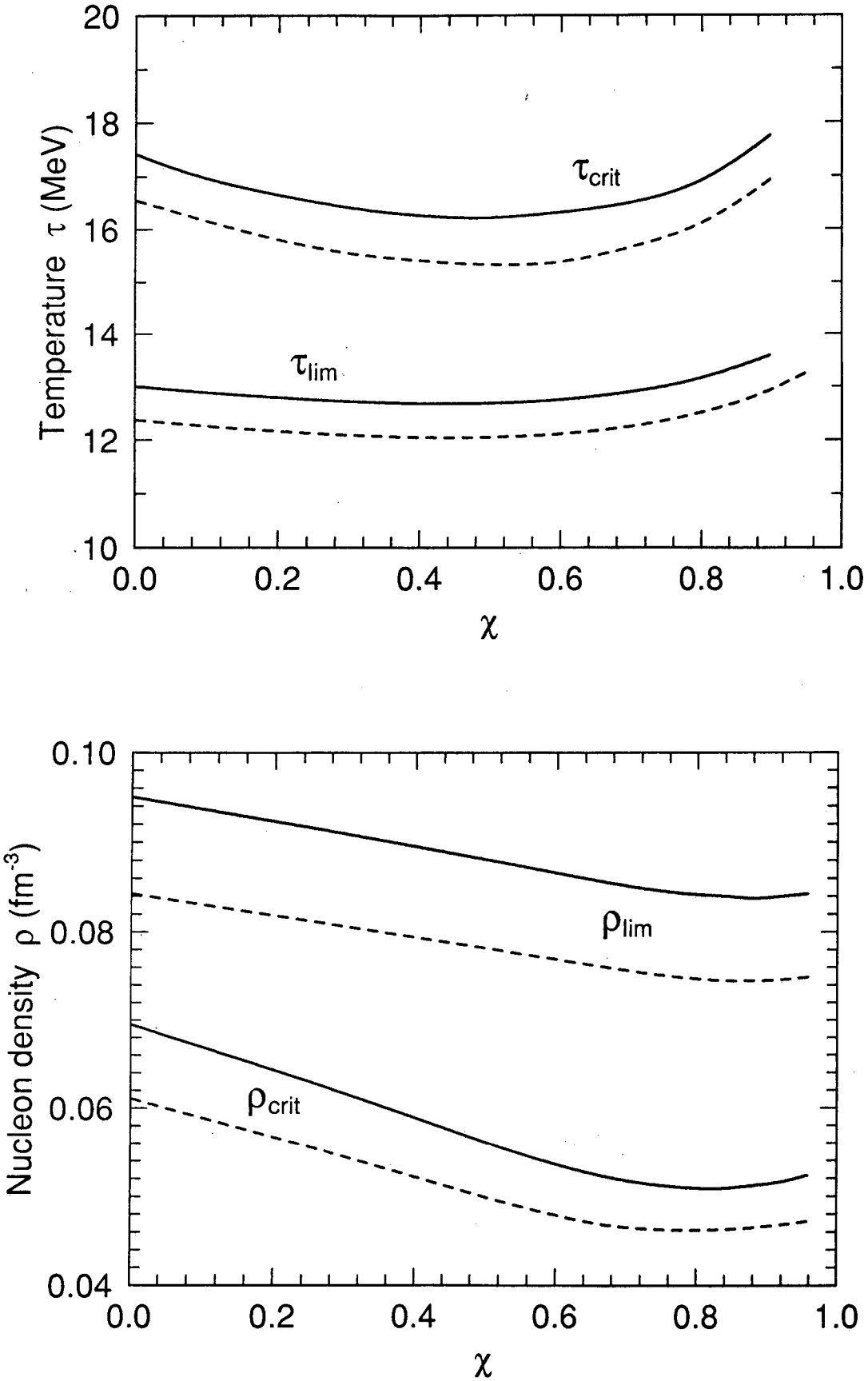
20
18
16
14
12
10
Temperature τ (MeV)
τcrit
τlim
0.0
0.2
0.4
0.6
0.8
1.0
χ
0.10
0.08
0.06
0.04
Nucleon density ρ (fm-3)
ρlim
ρcrit
0.0
0.2
0.4
0.6
0.8
1.0
χ

Figure 4

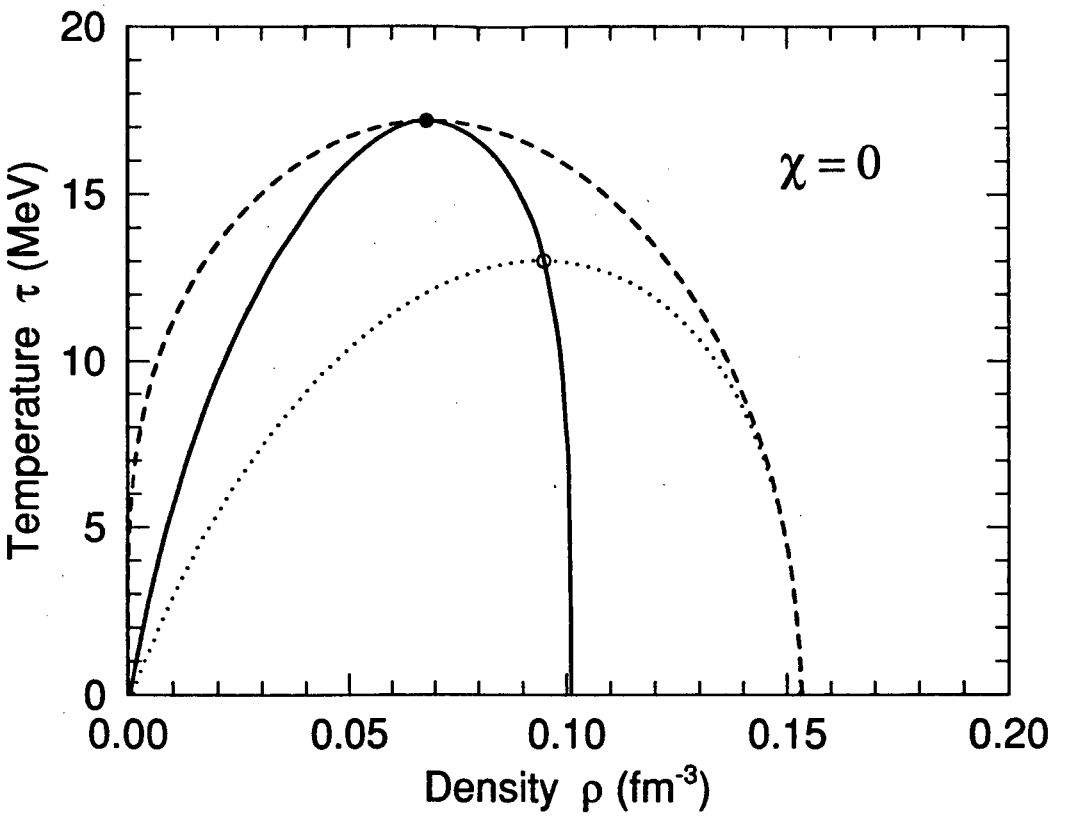
20
15
10
5
0
Temperature τ (MeV)
0.00
0.05
0.10
0.15
0.20
Density ρ (fm^{-3})
χ = 0

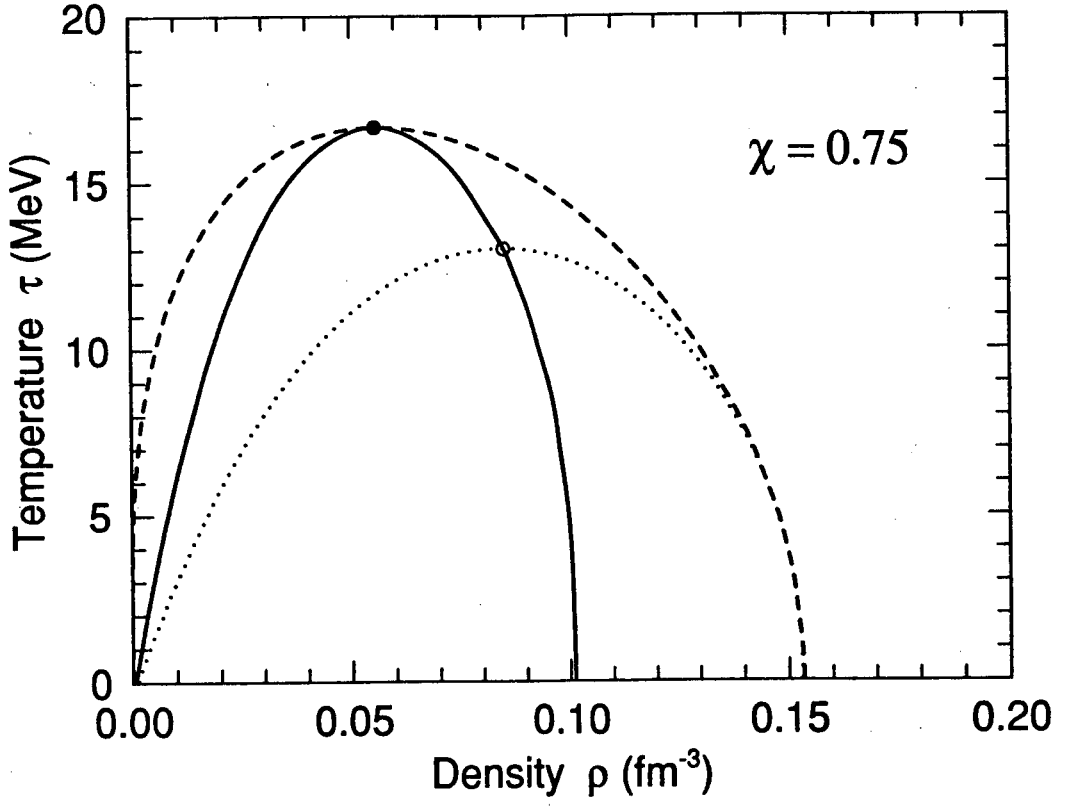
20
15
10
5
0
Temperature τ (MeV)
0.00
0.05
0.10
0.15
0.20
Density ρ (fm^{-3})
χ = 0.75

Figure 5

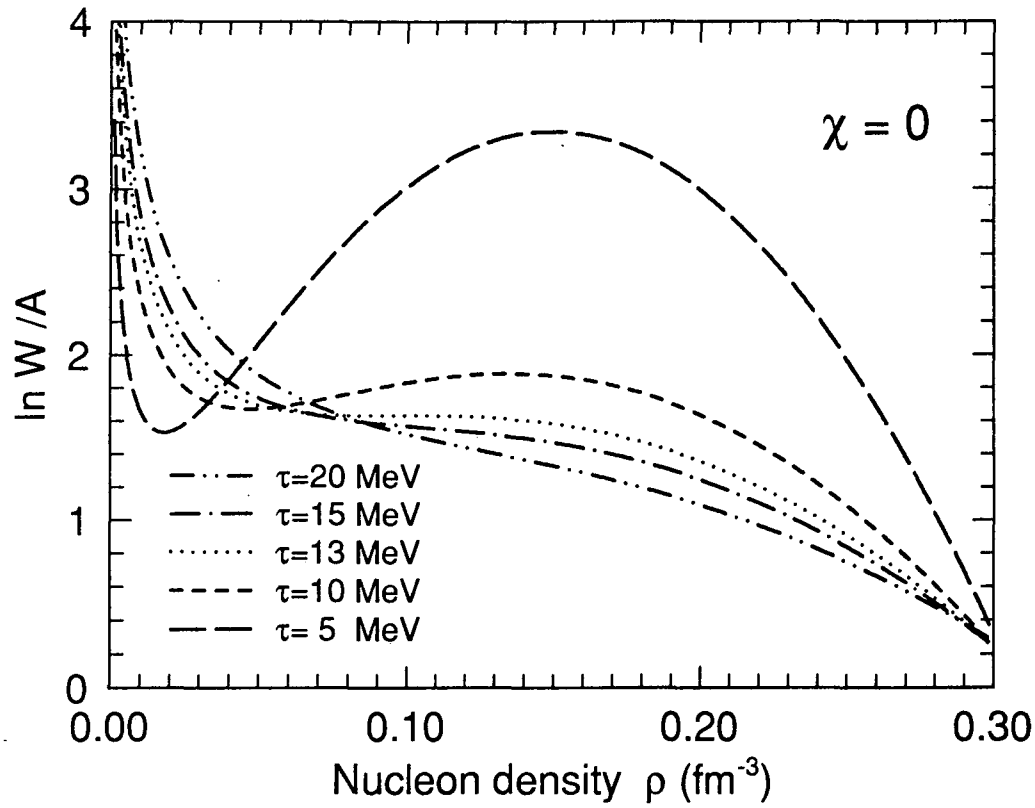
χ = 0
ln W /A
τ=20 MeV
τ=15 MeV
τ=13 MeV
τ=10 MeV
τ= 5 MeV
0
1
2
3
4
0.00
0.10
0.20
0.30
Nucleon density ρ (fm-3)

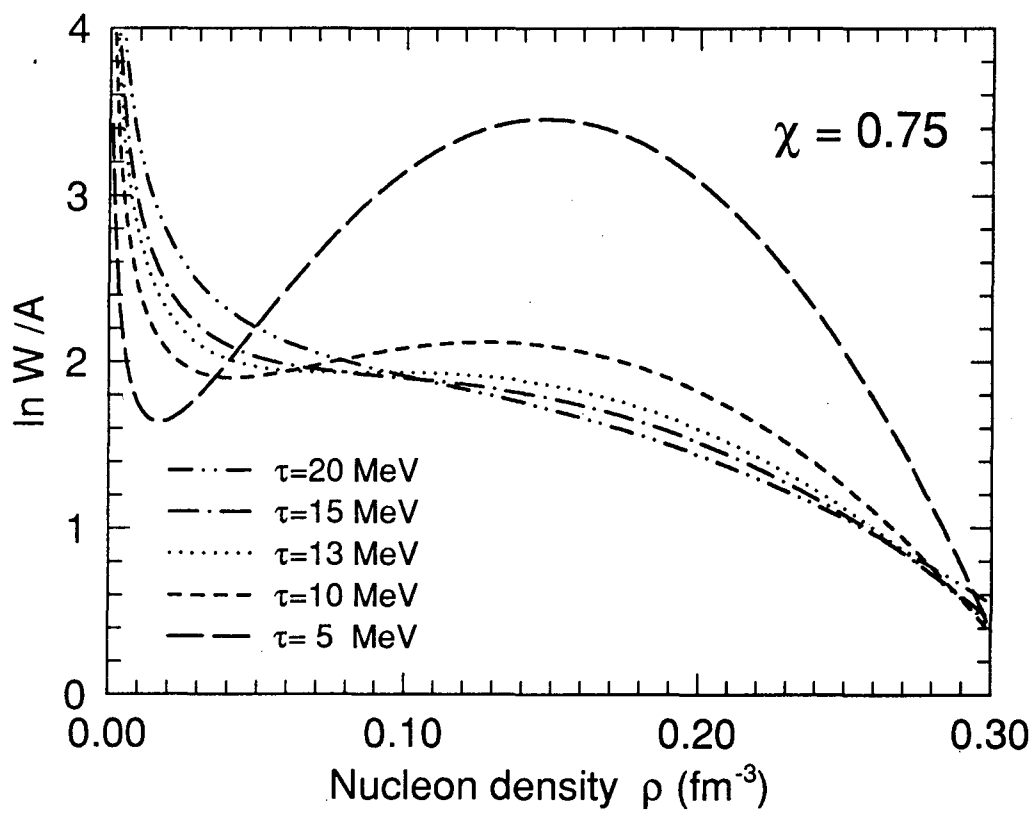
χ = 0.75
ln W /A
τ=20 MeV
τ=15 MeV
τ=13 MeV
τ=10 MeV
τ= 5 MeV
0
1
2
3
4
0.00
0.10
0.20
0.30
Nucleon density ρ (fm-3)

Figure 6

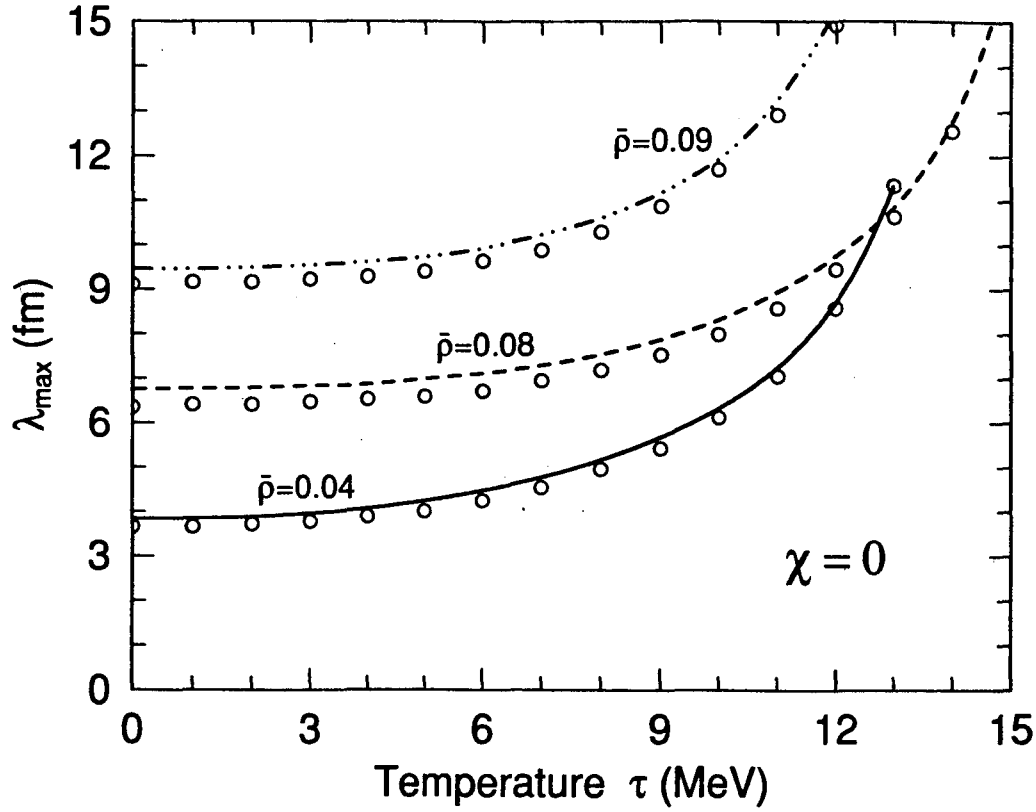
15
12
9
6
3
0
0
3
6
9
12
15
λ_{max} (fm)
Temperature τ (MeV)
$\bar{\rho}$=0.09
$\bar{\rho}$=0.08
$\bar{\rho}$=0.04
$\chi = 0$

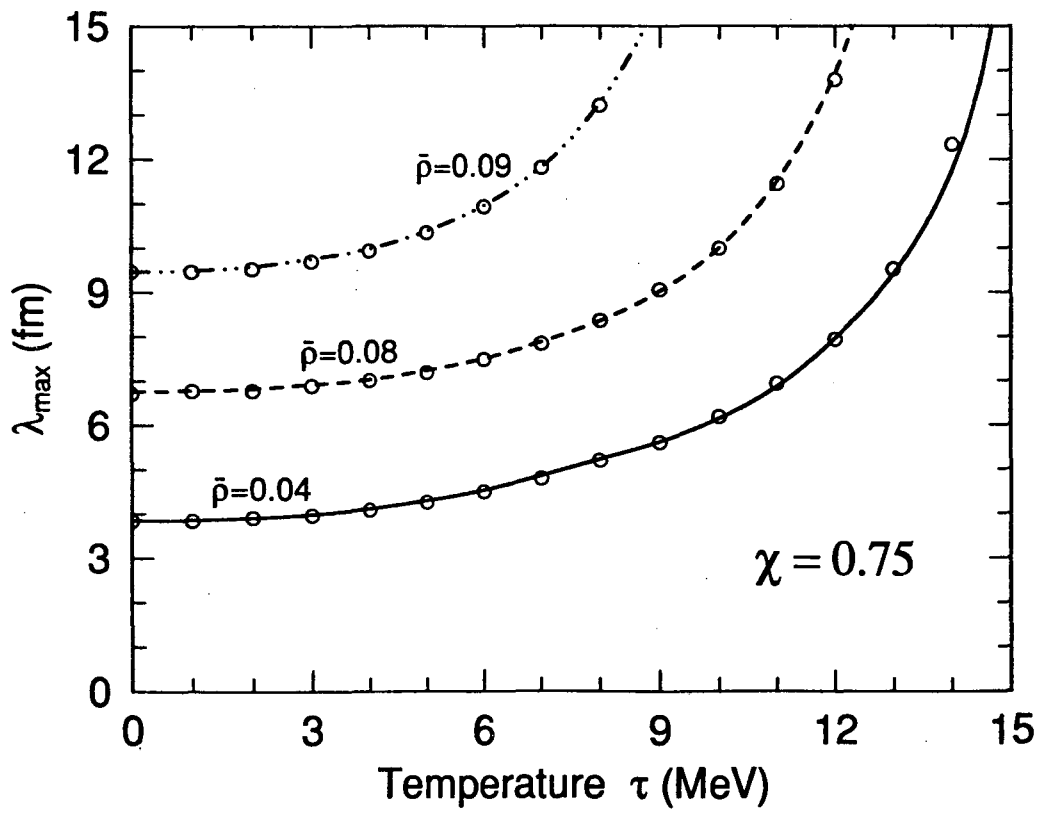
15
12
9
6
3
0
0
3
6
9
12
15
λ_{max} (fm)
Temperature τ (MeV)
$\bar{\rho}$=0.09
$\bar{\rho}$=0.08
$\bar{\rho}$=0.04
$\chi = 0.75$

Figure 7

LAWRENCE BERKELEY LABORATORY
UNIVERSITY OF CALIFORNIA
INFORMATION RESOURCES DEPARTMENT
BERKELEY, CALIFORNIA 94720